TECHNICAL REVIEW

NO. 1 – 2015

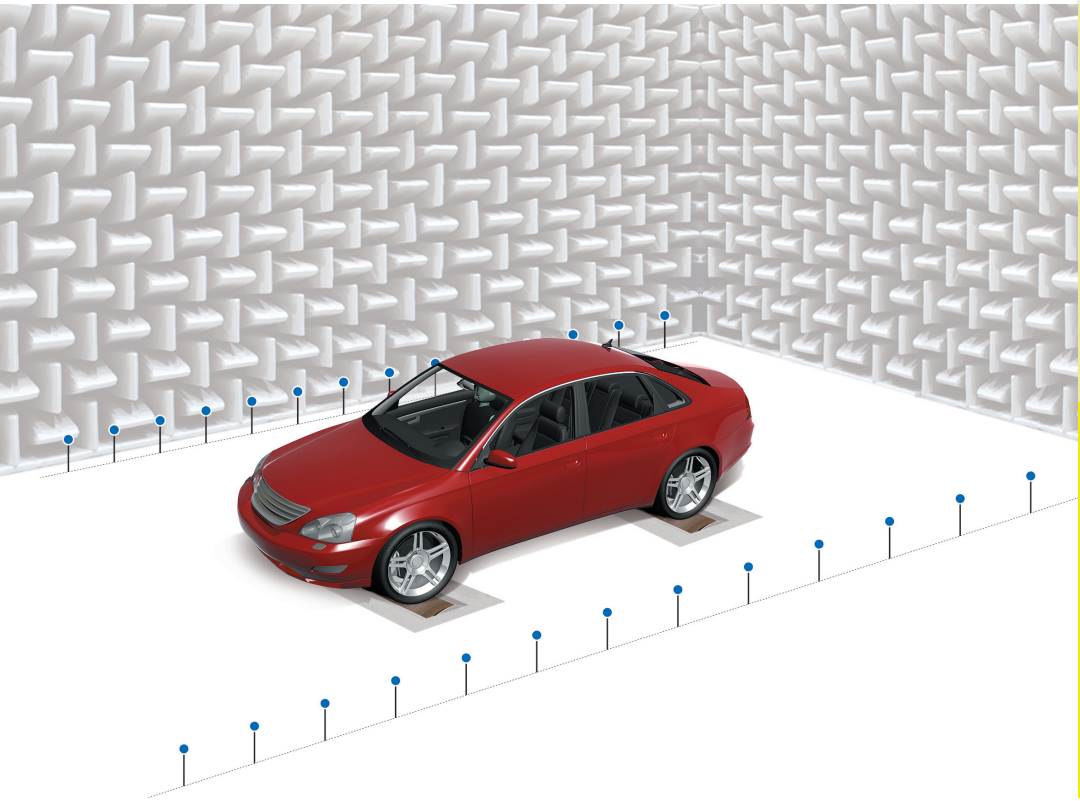

Fast Wideband Acoustical Holography

Evaluation of SPC and BSS for Indoor Pass-by Noise Contribution Analysis

Brüel & Kjær

BEYOND MEASURE

Previously issued numbers of Brüel & Kjær Technical Review

1 – 2014 Experimental Characterization of Operating Bladed Rotor Using HPS and SSI Techniques
Microphone Acoustic Impedence in Reciprocity Calibration

1 – 2013 Noise Test of Revised Notched Nozzle Using a Jet Engine
Heat Conduction Correction in Reciprocity Calibration of Laboratory Standard Microphones

1 – 2012 High-resolution Fly-over Beamforming
Clustering Approaches to Automatic Modal Parameter Estimation

1 – 2011 Performance Investigation of the Dual-Layer Array (DLA) at Low Frequencies
Calculating the Sound Field in an Acoustic Intensity Probe Calibrator – A Practical Utilisation of Boundary Element Modelling
Multi-field Microphone – When the Sound Field is Unknown

1 – 2010 Time Selective Response Measurements – Good Practices and Uncertainty
Measurement of Absorption Coefficient, Radiated and Absorbed Intensity on the Panels of a Vehicle Cabin using a Dual Layer Array with Integrated Position Measurement
ISO 16063 – 11: Uncertainties in Primary Vibration Calibration by Laser Interferometry – Reference Planes and Transverse Motion

1 – 2009 Use of Volume Velocity Sound Sources in the Measurement of Acoustic Frequency Response Functions
Turnkey Free-field Reciprocity System for Primary Microphone Calibration

1 – 2008 ISO 16063–11: Primary Vibration Calibration by Laser Interferometry: Evaluation of Sine Approximation Realised by FFT
Infrasound Calibration of Measurement Microphones
Improved Temperature Specifications for Transducers with Built-in Electronics

1 – 2007 Measurement of Normal Incidence Transmission Loss and Other Acoustical Properties of Materials Placed in a Standing Wave Tube

1 – 2006 Dyn-X Technology: 160 dB in One Input Range
Order Tracking in Vibro-acoustic Measurements: A Novel Approach Eliminating the Tacho Probe
Comparison of Acoustic Holography Methods for Surface Velocity Determination on a Vibrating Panel

1 – 2005 Acoustical Solutions in the Design of a Measurement Microphone for Surface Mounting
Combined NAH and Beamforming Using the Same Array
Patch Near-field Acoustical Holography Using a New Statistically Optimal Method

1 – 2004 Beamforming

1 – 2002 A New Design Principle for Triaxial Piezoelectric Accelerometers

(Continued on cover page 3)

Technical Review

No. 1 – 2015

Contents

Editor: Harry K. Zaveri

Fast Wideband Acoustical Holography

Jørgen Hald

Abstract

Patch near-field acoustical holography (NAH) methods like SONAH and ESM are limited to relatively low frequencies, where the average array-element spacing is less than half of the acoustic wavelength, while beamforming provides useful resolution only at medium-to-high frequencies. With adequate array design, both methods can be used with the same array. But for holography to provide good low-frequency resolution, a small measurement distance is needed, while beamforming requires a larger distance to limit side lobe issues. The wideband holography (WBH) method of the present paper was developed to overcome that practical conflict. Only a single measurement is needed at a relatively short distance and a single result is obtained covering the full frequency range. The method uses the principles of CS: A sparse sound field representation is assumed with a chosen set of basis functions, a measurement is taken with an irregular array, and the inverse problem is solved with a method that enforces sparsity in the coefficient vector. Instead of using regularization based on the 1-norm of the coefficient vector, an iterative solution procedure is used that promotes sparsity. The iterative method is shown to provide very similar results in most cases and to be computationally much more efficient.

Résumé

Les techniques d'holographie acoustique de champ proche (NAH) telles que SONAH et ESM ne valent que pour les fréquences relativement basses, l'espacement moyen entre les éléments de l'antenne étant inférieur à la moitié de la longueur de l'onde acoustique. La technique de formation de faisceau, pour sa part, ne fournit de bonne résolution que dans la plage des fréquences moyennes à élevées. Une même antenne, si elle est conçue de manière adéquate, peut servir à ces deux techniques. Toutefois, l'obtention d'une bonne résolution aux basses fréquences requiert une distance de mesurage courte, tandis que la technique de faisceau nécessite une distance plus importante afin de circonscrire les problèmes de lobes latéraux. La technique d'holographie acoustique bande large (WBH) présentée ici a été mise au point pour résoudre ce dilemme. Elle permet de se

satisfaire d'une seule mesure à une distance relativement courte, et la valeur obtenue couvre l'ensemble de la bande fréquentielle. Cette technique utilise les principes du "compressed sensing": une représentation parcimonieuse du champ acoustique est associée à un choix donné de fonctions, un mesurage est réalisé avec une antenne irrégulière, et le problème inverse est résolu au moyen d'une méthode qui renforce la parcimonie du vecteur de coefficient. Au lieu d'une régularisation basée sur la norme 1 de ce vecteur, c'est une procédure itérative qui est utilisée. Cette méthode s'est avérée produire des résultats très similaires dans la plupart des cas et être beaucoup plus efficace sur le plan des calculs.

Zusammenfassung

Patch-Methoden der akustischen Nahfeldholografie (NAH) wie SONAH und ESM sind auf relativ niedrige Frequenzen beschränkt, wobei der Abstand der Array-Elemente im Durchschnitt weniger als die halbe akustische Wellenlänge beträgt, während Beamforming nur bei mittleren bis hohen Frequenzen eine brauchbare Auflösung liefert. Bei entsprechendem Arrayaufbau können beide Methoden mit demselben Array angewendet werden. Um mit Holografie eine gute Auflösung im niedrigen Frequenzbereich zu erreichen, wird jedoch ein geringer Messabstand benötigt, während Beamforming einen größeren Abstand erfordert, um Probleme mit Nebenmaxima zu begrenzen. Die in diesem Artikel beschriebene Methode der Breitband-Holografie (WBH) wurde entwickelt, um diesen praktischen Konflikt zu überwinden. Sie erfordert nur eine einzige Messung in relativ kurzem Abstand und liefert ein Ergebnis, das den gesamten Frequenzbereich abdeckt. Die Methode verwendet das Prinzip des compressed sensing: Es wird eine dünnbesetzte Schallfeldrepräsentation mit einem gewählten Satz von Basisfunktionen angenommen. Die Messung erfolgt mit einem irregulären Array und das Inversenproblem wird mit einer Methode gelöst, die einen dünnbesetzten Koeffizientenvektor erzwingt. Anstelle einer Regularisierung auf Basis der Betragssummennorm des Koeffizientenvektors wird ein iteratives Lösungsverfahren verwendet, das Dünnbesetztheit begünstigt. Es wird gezeigt, dass das iterative Verfahren in den meisten Fällen sehr ähnliche Ergebnisse liefert und rechnerisch weitaus effizienter ist.

1. Introduction

Near-field acoustical holography (NAH) is based on performing 2D spatial discrete Fourier transforms (DFT), and therefore the method requires a regular

mesh of measurement positions. To avoid spatial aliasing problems, the mesh spacing must be somewhat less than half of the acoustic wavelength. In practice, this requirement sets a serious limitation on the upper frequency limit.

Some patch NAH methods, for example, the equivalent source method (ESM) [1] and statistically optimized NAH (SONAH) [2, 3], can work with irregular microphone array geometries, but still require an average array-element spacing less than half the wavelength. As described by Hald [4] this allows the use of irregular arrays that are actually designed for use with beamforming. Typically, good performance with beamforming can be achieved up to frequencies where the average array inter-element spacing is two to three wavelengths. A practical issue with such a solution is the fact that the patch NAH method requires measurement at a small distance to provide good resolution at low frequencies, while beamforming requires a medium-to-long distance to keep side lobes at low levels. So for optimal wideband performance, two measurements must be taken at different distances, and separate types of processing must be used with the two measurements, making it difficult to combine the results into a single result covering the combined frequency range.

The rather new compressed sensing (CS) methods have started making it possible to use irregular array geometries for holography up to frequencies where the average array inter-element spacing is significantly larger than half of the wavelength, see for example [5, 6, 7]. In general, CS techniques allow reconstruction of a signal from sparse irregular samples under the condition that the signal can be (approximately) represented by a sparse subset of expansion functions in some domain, that is, with the expansion coefficients of most functions equal to zero. Typically, the number of available samples is much smaller than the number of expansion functions, so the problem of determining the expansion coefficients is severely underdetermined. To obtain the correct solution, the solution method must enforce sparsity in the coefficient vector. This is typically done by somehow minimizing the 1-norm of the coefficient vector. In connection with acoustical holography, a set of elementary waves or elementary sources is used to represent the sound field in a given 3D region, and measurements are taken with an irregular array. Chardon and others [5] used a set of plane wave functions to represent the vibration of a planar star-shaped plate, while Hald [6, 7] used a set of monopole point sources. A key problem in basis-function selection is to make sure that a sufficiently sparse coefficient vector can represent the sound field with sufficient accuracy.

The present paper describes a new method called wideband holography (WBH), which was introduced in [6, 7], and which is covered by a pending patent [8]. The method is similar to the generalized inverse beamforming method published by Suzuki [9], which uses a source model in terms of monopole and multipole point sources, and which minimizes a cost function including the 1-norm of the coefficient vector. This minimization is performed by a special iterative algorithm. WBH uses as source model a mesh of monopole point sources with less than half wavelength spacing, and instead of minimizing the 1-norm of the coefficient vector to enforce sparsity, a dedicated iterative solver is used that promotes sparsity in a different way. A main contribution of the present paper is a comparison of results between WBH and a method that solves an optimization problem with 1-norm minimization. Section 2 outlines the basic theory. After an introduction to the applied array design in Section 3, results of different simulated measurements are presented in Section 4, and Section 5 contains results from real measurements. Finally, Section 6 contains the conclusions.

2. Theory

Input data for patch holography processing is typically obtained by simultaneous acquisition with an array of M microphones, indexed by $m = 1, 2, \ldots, M$, followed by averaging of the M by M element cross-power spectral matrix between the microphones. For the subsequent description, we arbitrarily select a single high-frequency line f with associated cross-power matrix $\mathbf{G}$. An eigenvector/eigenvalue factorization is then performed of that Hermitian, positive-semi-definite matrix $\mathbf{G}$:

$$\mathbf{G} = \mathbf{V}\mathbf{S}\mathbf{V}^H, \tag{1}$$

$\mathbf{V}$ being a unitary matrix with the columns containing the eigenvectors $\mathbf{v}_\mu$, $\mu = 1, 2, \ldots, M$, and $\mathbf{S}$ a diagonal matrix with the real non-negative eigenvalues s_μ on the diagonal. Based on the factorization in Eq. (1), the principal component vectors $\mathbf{p}_\mu$ can be calculated as:

$$\mathbf{p}_\mu = \sqrt{s_\mu}\,\mathbf{v}_\mu. \tag{2}$$

Just like ESM and SONAH, the WBH algorithm is applied independently to each of these principal components, and subsequently the output is added on a power

basis, since the components represent incoherent parts of the sound field. So for the subsequent description we consider a single principal component, and we skip the index μ, meaning that input data is a single vector **p** with measured complex sound pressure values.

WBH uses a source model in terms of a set of elementary sources or wave functions and solves an inverse problem to identify the complex amplitudes of all elementary sources. The source model then applies for 3D reconstruction of the sound field. Here we will consider only the case where the source model is a mesh of monopole point sources retracted to be behind/inside the real/specified source surface, that is, similar to the model applied in ESM [1]. Figure 1(a) shows a typical setup for patch ESM, where a planar array covers a patch of the source surface, and a monopole source model inside the source surface extends somewhat beyond the measurement area. Figure 1(b) shows an alternative configuration of the equivalent sources that avoids the need for a 3D source surface geometry: A planar mesh of monopoles parallel with the array is retracted some small distance inside the real source surface and covers an area slightly larger than the array.

Fig. 1. Illustration of two alternative setups for patch ESM

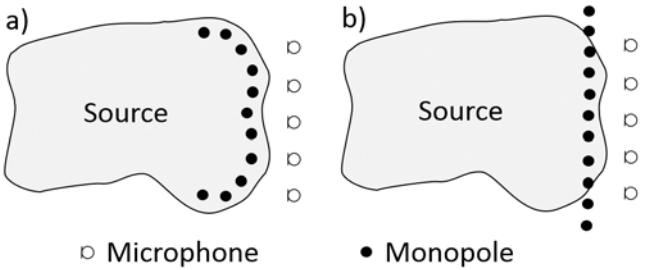

With A_{mi} representing the sound pressure at microphone m due to a unit excitation of monopole number i, the requirement that the modelled sound pressure at microphone m must equal the measured pressure p_m can be written as:

$$p_m = \sum_{i=1}^{I} A_{mi}\, q_i \,. \tag{3}$$

Here, I is the number of point sources, and q_i , $i = 1, 2, \ldots, I$, are the complex amplitudes of these sources. Equation (3) can be rewritten in matrix-vector notation as:

$$\mathbf{p} = \mathbf{A}\mathbf{q}\,, \tag{4}$$

where $\mathbf{A}$ is an M by I matrix containing the quantities A_{mi}, and $\mathbf{q}$ is a vector with elements q_i. In CS terminology the matrix $\mathbf{A}$ is called the sensing matrix.

When doing standard patch holography calculations using ESM, Tikhonov regularization is typically applied to stabilize the minimization of the residual vector $\mathbf{p}$-$\mathbf{Aq}$. This is done by adding a penalty proportional to the 2-norm of the solution vector when minimizing the residual norm:

$$\underset{\mathbf{q}}{\text{Minimize}} \left\|\mathbf{p} - \mathbf{A}\mathbf{q}\right\|_2^2 + \theta^2 \left\|\mathbf{q}\right\|_2^2 . \tag{5}$$

A very important property of that problem is the fact that it has the simple analytic solution:

$$\mathbf{q} = \left[\mathbf{A}^H\mathbf{A} + \theta^2\mathbf{I}\right]^{-1} \mathbf{A}^H\mathbf{p}, \tag{6}$$

where $\mathbf{I}$ is a unit diagonal matrix, and H represents Hermitian transpose. A suitable value of the regularization parameter θ for given input data $\mathbf{p}$ can be identified automatically, for example, by use of generalized cross-validation (GCV), see Gomes and Hansen [10]. When using a specific irregular array well above the frequency of half wavelength average microphone spacing, the system of linear equations in Eq. (4) is in general strongly underdetermined, because the monopole mesh must have spacing less than half of the wavelength, that is, much finer than the microphone grid. During the minimization in Eq. (5), the undetermined degrees of freedom will be used to minimize the 2-norm of the solution vector. The consequence is a reconstructed sound field that matches the measured pressure values at the microphone positions, but with minimum sound pressure elsewhere. Estimates of, for example, sound power will therefore be much too low. Another effect is ghost sources that help focus radiation towards the microphones. This will be illustrated by simulated measurements.

If the true source distribution is sparse (with a majority of elements in $\mathbf{q}$ equal to zero), or close to sparse, the above phenomena can be alleviated by replacing the 2-norm in the penalty term of Eq. (5) by a 1-norm:

$$\underset{\mathbf{q}}{\text{Minimize}} \left\|\mathbf{p} - \mathbf{A}\mathbf{q}\right\|_2^2 + \theta^2 \left\|\mathbf{q}\right\|_1 , \tag{7}$$

see for example [5] and [9]. The minimization of the 1-norm of the solution vector will have the effect of favoring sparse solutions. Important problems related to this formulation are the lack of an analytic solution and the fact that no good tool is available to identify an optimal value of the regularization parameter θ for given input data $\mathbf{p}$. An equivalent problem was solved by Chardon and others [5]:

$$\underset{\mathbf{q}}{\text{Minimize}} \; \|\mathbf{q}\|_1 \text{ subject to } \|\mathbf{p} - \mathbf{A}\mathbf{q}\|_2 \leq \delta. \tag{8}$$

Here, however, the parameter δ is difficult to determine. In cases where the applied source model cannot represent the full measured sound field (for example due to sources outside the measurement region or reflections), a rather large value of δ may be needed for the problem to be solvable. Instead of requiring a small 2-norm of the residual vector,

$$\mathbf{r}(\mathbf{q}) \equiv \mathbf{p} - \mathbf{A}\mathbf{q}, \tag{9}$$

we can alternatively require a solution close to a minimum of the squared residual function F,

$$F(\mathbf{q}) \equiv \tfrac{1}{2}\|\mathbf{r}(\mathbf{q})\|_2^2 \;=\; \tfrac{1}{2}\|\mathbf{p} - \mathbf{A}\mathbf{q}\|_2^2 \;. \tag{10}$$

Such a minimum will be characterized by the gradient vector $\nabla F(\mathbf{q})$,

$$\nabla F(\mathbf{q}) \;=\; -\mathbf{A}^H(\mathbf{p} - \mathbf{A}\mathbf{q}), \tag{11}$$

having a small norm. Thus, instead of Eq. (8), we solve the problem:

$$\underset{\mathbf{q}}{\text{Minimize}} \; \|\mathbf{q}\|_1 \text{ subject to } \|\nabla F\mathbf{q}\|_2 = \left\|\mathbf{A}^H(\mathbf{p} - \mathbf{A}\mathbf{q})\right\|_2 \leq \delta \,. \tag{12}$$

The optimization problem of Eq. (12) is convex and can be solved by available Matlab libraries. In the present paper the CVX library has been used, see [5, 11], so the method will just be called CVX. The computational demand is, however, significantly higher than for the Tikhonov problem in Eq. (5) because no analytic

solution exists. According to experience, a good way of defining the parameter δ in Eq. (12) is:

$$\delta = \varepsilon \left\| \nabla F(\mathbf{q} = \mathbf{0}) \right\|_2 = \varepsilon \left\| \mathbf{A}^H \mathbf{p} \right\|_2 , \tag{13}$$

where ε is a small number. Its value must be chosen small enough to guarantee that we get close to a minimum, but large enough that we do not enforce a modelling of measurement noise/errors. The requirement on the gradient norm in Eq. (12) occurs also in the stopping criterion of the iterative solution method implemented in WBH, see Eq. (14) below, but only as one of several conditions that will imply stopping.

A main idea behind the iterative WBH algorithm is to remove/suppress the ghost sources associated with the real sources in an iterative solution process, starting with the strongest real sources. WBH applies a steepest descent iteration to minimize the quadratic residual function $F(\mathbf{q})$, see Appendix A for details. In the first step, a number of real as well as ghost sources will appear in $\mathbf{q}$. When using irregular array geometries, the ghost sources will in general be weaker than the strongest real source(s). We can therefore suppress the ghost sources by setting all components in $\mathbf{q}$ below a certain threshold to zero. The threshold is computed as being a number of decibels D below the amplitude of the largest element in $\mathbf{q}$. Initially, D is set to a very small value D_0, and it is then increased during the iteration, typically by the same number of decibels ΔD in every step. Typical values are $D_0 = 0.1$ and $\Delta D = 1$. The dynamic range limitation will gradually disappear during the iteration, so it has the role of steering the iteration towards a sparse solution in its initial phase.

Figure 2 contains a block flowchart diagram for the iteration, which is stopped when:

$$D > D_{\max} \quad \text{or} \quad \left\| \nabla F(\mathbf{q}) \right\|_2 \le \varepsilon \left\| \nabla F(\mathbf{0}) \right\|_2 = \varepsilon \left\| \mathbf{A}^H \mathbf{p} \right\|_2 , \tag{14}$$

where $D_{\max}$ is an upper limit on D and ε is a small number. The following values have been found to work in general very well: $D_{\max} = 60$ and $\varepsilon = 0.01$. Typically, the steepest descent method has very slow final convergence because of zigzagging, and therefore the first of the two criteria in Eq. (14) will usually be

Fig. 2. Flow chart of the modified steepest descent algorithm used in WBH

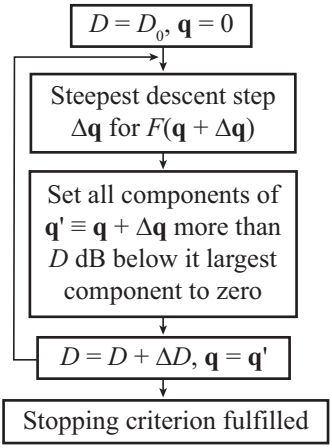

fulfilled first. $D_{\max}$ can be changed to match the quality of data, but the choice does not seem to be critical. $D_{\max} = 60$ has been found to support the identification of weak sources, even when measurements are slightly noisy. Larger values do not seem to improve much. Smaller values may be required for very noisy data.

Starting with only 0.1 dB dynamic range means that only the very strongest source(s) will be retained, while all related ghost sources will be removed. When we use the dynamic range limited source vector as the starting point for the next iteration, the components of the residual vector related to the very strongest source(s) have been reduced, and therefore the related ghost sources have been reduced correspondingly. Increasing the dynamic range will then cause the next level of real sources to be included, while suppressing the related ghost sources, etc.

After the termination of the above algorithm based on steepest descent directions, a good estimate of the basic source distribution has been achieved. The typical zigzagging progress in the last steepest descent steps means that often the direction given as the sum of the last two steps will support good progress. The step-size that minimizes the quadratic function $F(\mathbf{q})$ along that direction can be calculated analytically, and that so-called extrapolation step is used as part of WBH in the present work.

A few conjugate gradient iteration steps without dynamic range limitation can then optionally be performed to ensure convergence to a point very close to a minimum of $F(\mathbf{q})$. See Appendix B for details on the algorithm. Usually, the

effect on the source model and the modelled sound field is relatively small, because the primary steepest descent algorithm has already reduced the residual to be close to a minimum. However, it ensures that full convergence has been achieved. The stopping criteria used with the conjugate gradient iteration are:

$$\left\|\nabla F(\mathbf{q}+\Delta\mathbf{q})\right\|_2 < \varepsilon\left\|\mathbf{A}^H\mathbf{p}\right\|_2 \quad \text{or} \quad \left\|\nabla F(\mathbf{q}+\Delta\mathbf{q})\right\|_2 > \left\|\nabla F(\mathbf{q})\right\|_2, \tag{15}$$

where $\Delta\mathbf{q}$ is the latest step. In comparison with the CVX method defined in Eq. (12) and Eq. (13) notice that selection of too small a value of ε will not prevent termination of the conjugate gradient algorithm of WBH. In that case it will stop when the gradient norm starts increasing. When that happens, the last step is discarded.

The WBH algorithm, which enforces a maximum degree of sparsity in the source distribution, has been found to work well at high frequencies, when a suitable irregular array is used at not too small a measurement distance. However, at low frequencies WBH easily leads to misleading results, when two compact sources are so closely spaced that available data does not support a resolution of the two. In that case, the WBH algorithm will often identify a single compact source at a position between the two real sources, so the user might be drawing wrong conclusions about the root cause of the noise. Use of the traditional Tikhonov regularization of Eq. (6), that is, a standard ESM algorithm, will in that case typically show a single large oblong source area covering both of the two real sources. To minimize the risk of misleading results, it is recommended to use the standard ESM solution up to a transition frequency at approximately 0.7 times the frequency of half wavelength average array inter-element spacing (that is, spacing ≈ 0.35λ), and above that transition frequency switch to the use of WBH. This is illustrated by the simulated measurement in Section 4.B, where it is shown that the CVX method exhibits similar behavior, so it should probably also be supplemented by typically the ESM algorithm at low frequencies.

It is quite easy to show that the first steepest descent direction $\Delta\mathbf{q}$ (see Figure 2) is equivalent to a delay and sum (DAS) beamforming map, which has poor low-frequency resolution. The first source identified by WBH will therefore be located at the peak of a DAS map, which in this case is somewhere between the two real sources. At higher frequencies, DAS has good resolution, so therefore the problem of separate sources being replaced by a single central source is probably acceptable above the transition frequency described above.

3. Array Design

As described in the introduction, the method of the present paper follows the principles of CS, being based on measurements with a random or pseudo-random array geometry in combination with an enforced sparsity of the coefficient vector of the source model. The array geometry used in the simulated measurements of the present paper is shown in Figure 3. It has 12 microphones uniformly distributed in each one of five identical angular sectors. The average element spacing is approximately 12 cm, implying a low-to-high transition frequency close to 1 kHz (where 0.35λ is close to 12 cm). The geometry has been optimized for minimum side lobe level with DAS beamforming measurements up to 6 kHz as described in [4]. This optimization guarantees a maximum ability of the array to distinguish plane waves incident from different directions. If the measurement distance is not too short, the ability to distinguish point sources in different directions will also be good.

Fig. 3. Geometry of the applied planar pseudo-random 60-element microphone array with 1 m diameter

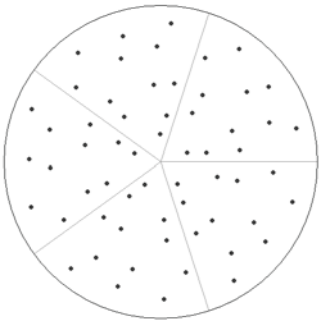

An important finding from simulated measurements with the chosen array design is that the measurement distance should not be shorter than approximately a factor two times the average microphone spacing for the method to work well at the highest frequencies. A factor of three is even better, and distances up to typically 0.7 times the array diameter work fine. When the measurement distance is increased, each source in the WBH source model will expose the microphones over a wider area, increasing the ability of the irregular array to distinguish different sources. To get acceptable low-frequency resolution, however, the measurement distance should not be too long either, so overall the best distance seems to be two to three times the average array inter-element spacing.

4. Simulated Measurements

All CVX and WBH calculations in the present paper were performed using $D_0 = 0.1$, $\Delta D = 1.0$, $D_{\max} = 60$ and $\varepsilon = 0.01$.

4.A Single monopole point source

The aim of the single-monopole simulated measurement is to demonstrate: i) What happens if Tikhonov regularization is applied above the frequency of half wavelength average array element spacing, and ii) how much and which kind of improvement is achieved by applying the sparsity promoting CVX and WBH algorithms.

Fig. 4. Setup for simulated measurement on a single monopole point source

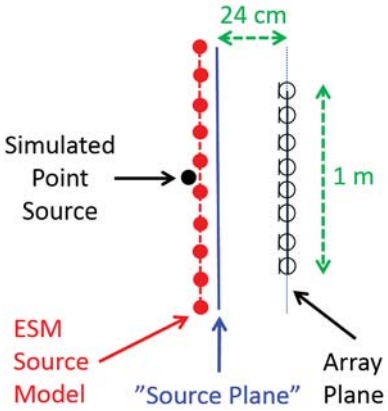

As illustrated in Figure 4, we consider a setup with a monopole point source located on the array axis at 28 cm distance from the array plane, while the source-model mesh is at 27 cm distance, and the sound field in reconstructed in a "source plane" 24 cm from the array plane. The reconstruction mesh has 51 columns and 51 rows with 2 cm spacing, covering a 1 m × 1 m area centered on the array axis. The source-model mesh is similar, that is, with 2 cm spacing, but it is extended by six rows/columns in all four directions. In total, 63 × 63 = 3969 complex point-source amplitudes must be determined from the 60 measured complex sound-pressure values. No measurement errors/noise was added.

The left column of Figure 5 shows the 4 kHz sound intensity maps on the source plane, while the right column shows the corresponding sound pressure maps on the measurement plane. From the top and downwards the true maps are shown, followed by the reconstructions using Tikhonov regularization (using 20 dB

Fig. 5. Results from a simulated measurement on a single monopole point source. All plots in a column have equal scaling

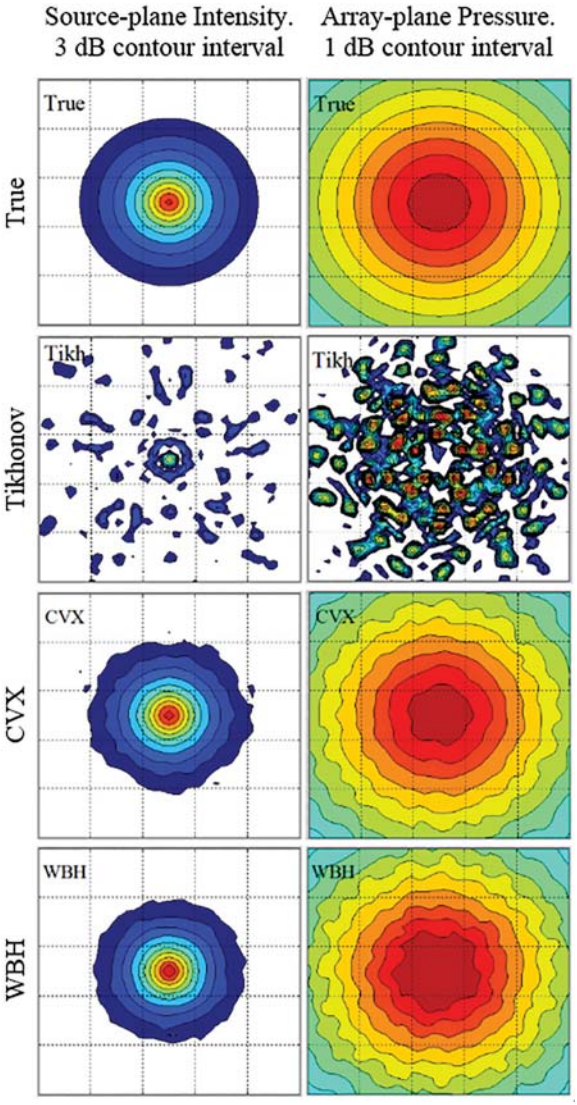

dynamic range), CVX and at the bottom WBH. The CVX and WBH maps are both very close to the true maps, as could be expected in the present case, where the source-model plane is only 1 cm from the monopole point source. The sound intensity reconstruction based on Tikhonov regularization shows a small low-level peak at the true source position, but in addition, there are quite a lot of ghost sources. These ghost sources are responsible for focusing the modelled sound field towards the microphones to produce the measured pressure at these positions with a minimum of radiated power. This is evident from the map of the sound pressure in the array plane.

Fig. 6. Estimated sound power spectra relative to the true sound power spectrum. All spectra were obtained by area integration of the intensity maps in Figure 5

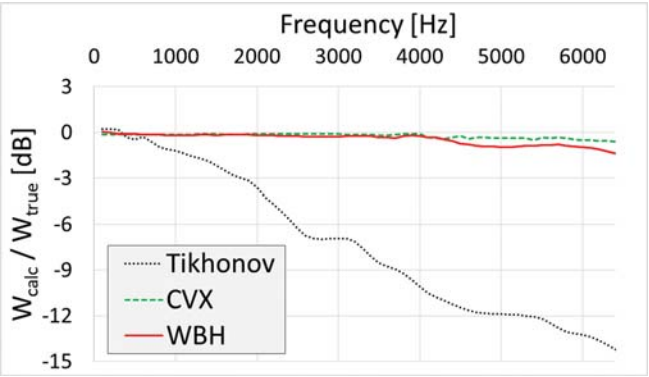

Area integration of sound intensity maps like those in Figure 5 leads to the sound power spectra compared in Figure 6. Here, the spectra from the three reconstruction methods have been normalized by the spectrum from the true intensity map. CVX and WBH produce accurate sound power estimates over the entire range from 100 Hz to 6.4 kHz, while Tikhonov regularization leads to acceptable accuracy up to approximately 1 kHz. Above that frequency, an increasing underestimation is observed due to the increasing ability of the source model to establish the measured pressure at the microphones and low pressure in all other directions. Calculation times for the 64 frequencies represented in Figure 5, using Matlab implementations of the CVX and WBH methods, were 829 s for CVX and 32 s for WBH.

4.B Two coherent, in-phase monopole sources of equal level

The aim of this simulated measurement is to demonstrate some important resolution properties at low frequencies. For that purpose, we use a set-up similar

Fig. 7. True and reconstructed sound intensity maps for two coherent, in-phase monopole sources of equal amplitude. All plots have 1.5 dB contour interval, but different thresholds. The area-integrated sound power is almost identical for all plots

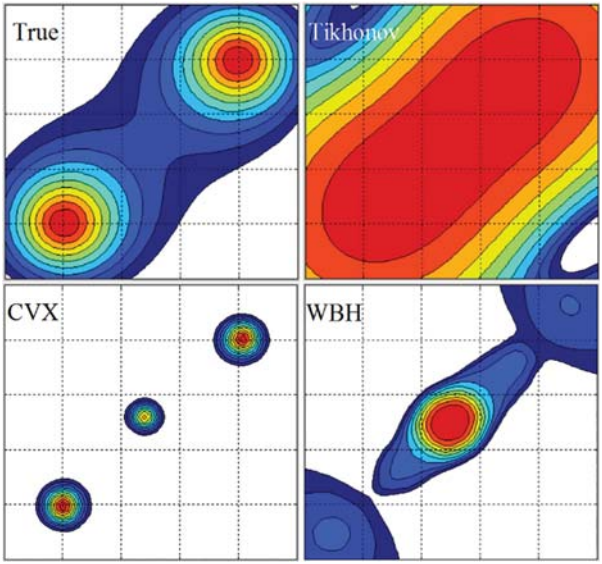

to that of Fig. 4, but with two sources within a mapping area of half the dimensions. The two monopole point sources are located 29 cm in front of the array plane at (x,y) coordinates (15,15) cm and (-15,-15) cm relative to the array axis, while the source-model mesh is at a distance of 25.5 cm, and the sound field is reconstructed in a "source plane" 24 cm from the array plane. Thus, in this case, the real sources are 3.5 cm behind the source model. The reconstruction mesh has 51 columns and 51 rows with 1 cm spacing, covering a 0.5 m × 0.5 m area centered on the array axis, and the source-model mesh is similar, that is, with 1 cm spacing, but it is extended by six rows/columns in all four directions. Random noise was added to the complex microphone pressure data at a level 30 dB below the average sound pressure across the microphones.

Figure 7 shows sound intensity maps at 400 Hz. The top row contains to the left the true intensity and to the right the intensity obtained using Tikhonov regularization with 20 dB dynamic range. With the applied combination of source separation, measurement distance and dynamic range, the two sources are not resolved when using Tikhonov, although it is close. The map indicates, however, the shape of the source distribution. The bottom row contains to the left the CVX

reconstruction and to the right the WBH result. Both methods put a concentrated false source in the middle between the two real sources plus two sources close to the real sources. This phenomenon, which is strongest for WBH, could lead to wrong conclusions about the origin of the measured noise. So as described at the end of Section 2 it is recommended to have at least an option for use of standard ESM (with Tikhonov regularization) at the low frequencies instead of CVX or WBH.

4.C Two coherent, in-phase monopole sources with 10 dB level difference

A main purpose of this section is to investigate the ability of the CVX and WBH methods to identify weak sources in the presence of strong ones. We use the same set-up as in the above Section 4.B, except that the lower left source (Source 2) is now assigned an excitation 10 dB below that of the upper right source (Source 1). Figure 8 shows the true and the reconstructed sound intensities on the "source plane" at 5 kHz with a 20 dB display range. The two sources are well identified by both CVX and WBH, and the two methods show very similar results. The maps actually look much the same at all frequencies between 1 kHz and 5 kHz. Sound power integration areas are shown with line style corresponding to the associated sound power spectra in Figure 9. Except for the weak source (Source 2) at the lowest frequencies, the two reconstruction methods estimate almost the same sound power spectra for the two sources. As described above, a standard ESM algorithm should be used anyway at the lowest frequencies – for the present array up to 1 kHz. The apparent small overestimation of the sound power for Source 1 up to around 4 kHz is probably instead an underestimation of the true power. The true intensity map is smoother and therefore some of the power of Source 1 will be outside the associated integration area. Apart from a 2.5 dB dip around 4 kHz in the estimated power for Source 2, the accuracy is good up to around 5 kHz, and above that frequency, an increasing underestimation is observed. The maximum frequency of the present array (with 12 cm average microphone spacing) in connection with the SONAH and ESM algorithms is approximately 1.2 kHz, so apparently the CVX and WBH methods extend the frequency range by a factor of around 4.

The calculation times for the 32 frequencies represented in Figure 9 were 490 s for CVX and 16 s for WBH, so again WBH is faster by approximately a factor of 30. Another advantage of WBH is the already mentioned smaller sensitivity of WBH to the specified target reduction in the gradient norm: Too small a value of ε causes the CVX method to become unstable.

Fig. 8. True and reconstructed sound intensities in the "source plane". Display range is 20 dB with 2 dB contour interval. All three plots use the same scale. Source 1 is the stronger source in the upper right corner

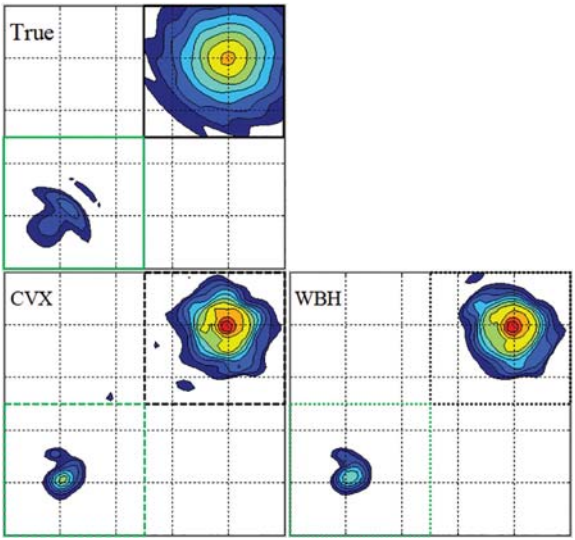

Fig. 9. Area-integrated sound power spectra for the areas of Figure 8

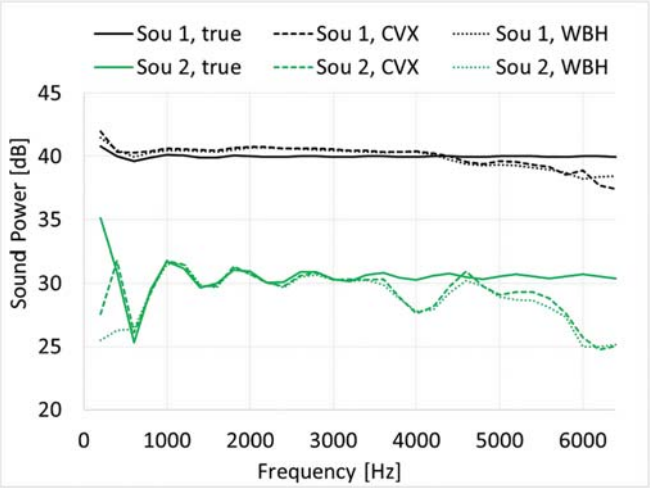

4.D Plate in a baffle

Fig. 10. Contour plots at 3 and 4 kHz of sound intensity in the reconstruction plane 1 cm above the plate. Display range is 20 dB with 2 dB contour interval. For each frequency, the same scale is used

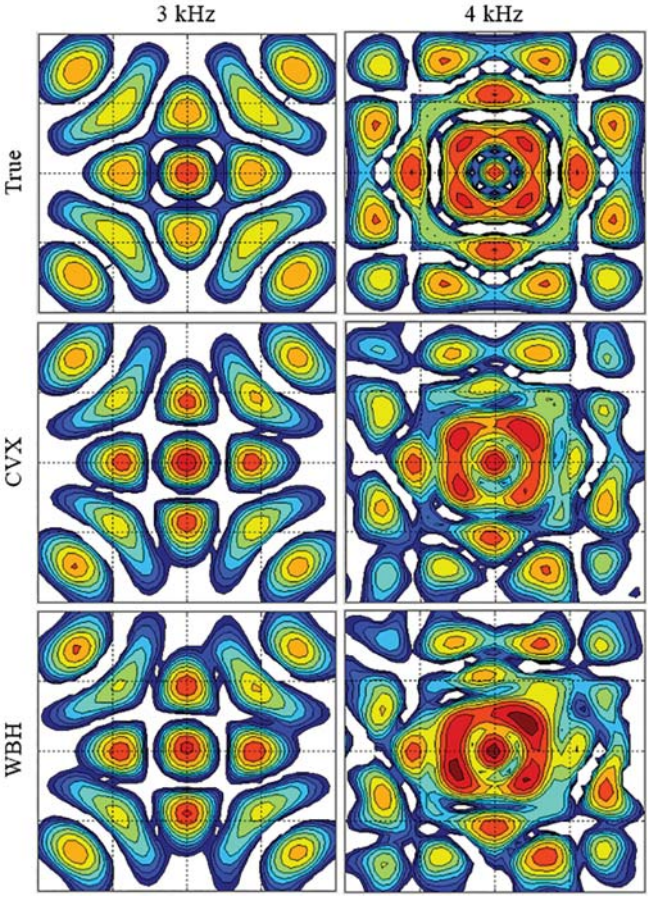

The aim of the simulated plate measurements is to show that both the CVX and the WBH methods can give quite good results even when the true source distribution is not sparse. As an example of a more distributed source, a baffled, center-driven, simply supported, 6 mm thick, 40 cm × 40 cm aluminum plate has been used. The coincidence frequency for the plate is at 2026 Hz. The vibration

pattern was calculated using the formulation by Williams [12], and subsequently the radiated sound field was obtained using the discretized Rayleigh integral, approximating the plate velocity distribution by 161 × 161 monopole point sources. This allowed the microphone sound-pressure values and the "true" pressure and particle velocity in a reconstruction plane 1 cm above the plate to be calculated. As for the simulated measurements on two monopole point sources, random noise was added to the complex microphone pressure data at a level 30 dB below the average sound pressure across the microphones. The reconstruction mesh had 41 × 41 points with 1 cm spacing, covering exactly the plate area, and the array was placed 24 cm above the plate. For the WBH sound field reconstruction a source model comprising 53 × 53 monopole point sources with 1 cm spacing was located 1 cm below the plate.

Figure 10 shows the true sound intensity and the corresponding CVX and WBH reconstructions at 3 and 4 kHz with a 20 dB display range. Overall, the reconstruction is good, with a little too high weight on the central area, the two methods performing again equally well. At 4 kHz the reconstructed intensity patterns start getting distorted, because the complexity of the vibration pattern becomes too high in relation to the data provided by the array. As mentioned earlier, the reconstruction accuracy at the highest frequencies can be improved by an increase of the measurement distance up to three times the array inter-element spacing, but, of course, at the expense of slightly poorer low-frequency resolution.

Fig. 11. Reconstructed relative to true sound power of the plate in decibels. All power values were obtained by area integration of maps like those in Figure 10

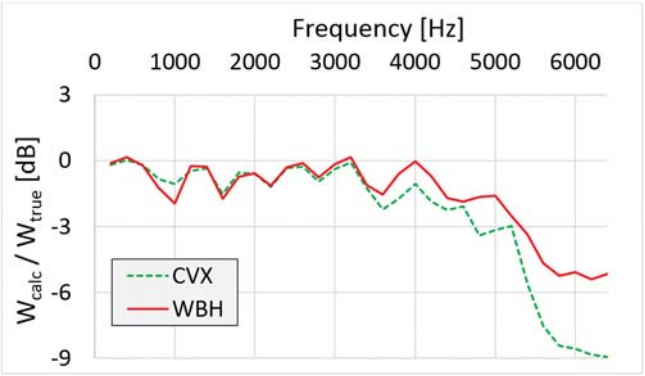

Figure 11 shows the relative sound power spectrum of the CVX and WBH reconstructions: At each frequency, the reconstructed and true sound intensity maps (as shown in Figure 10) have been area integrated over the entire plate, and

the ratio between the estimated and the true sound power values have been plotted in decibels. There is a consistent small underestimation, but up to 5 kHz it remains within 2 dB. Above 5 kHz the underestimation increases rapidly, in particular for the CVX based algorithm. The calculation time for the 32 frequencies represented in Figure 11 was 238 s for CVX and 9 s for WBH.

5. Real Measurement on Two Small Loudspeakers

Figure 12 shows two Brüel & Kjær mouth simulators, Type 4227, set up 36 cm from the array and with 12 cm separation between the two sources. Thus, the measurement distance has been increased to three times the average microphone spacing. The two sources were excited from two independent stationary-random white-noise generators adjusted to equal levels. Beyond the array measurement, a scan was also performed with a two-microphone sound intensity probe across a plane 7 cm from the two sources. 13 × 6 positions with 3 cm spacing were measured, covering an area of 36 cm × 15 cm. The measurements were performed in a normal room with no acoustical treatment.

Fig. 12. 60-channel array at 36 cm distance from two Brüel & Kjær mouth simulators, Type 4227

The array measurement consisted in simultaneously recording 10 seconds of time data with 12.8 kHz bandwidth from all array microphones. As described in Section 2, the processing started with averaging of the 60 × 60 element cross-spectral matrix between all array microphones. Then, a principal component decomposition of that matrix was performed, and the WBH algorithm was applied to each significant component. In the present case of two independently excited sources, there were two such significant principal components. The planar WBH reconstruction mesh was in a source plane parallel with the array plane and

*Fig. 13. Sound intensity maps from WBH for the 1/3-octave bands 4 kHz **(left)** and 5 kHz **(right)***

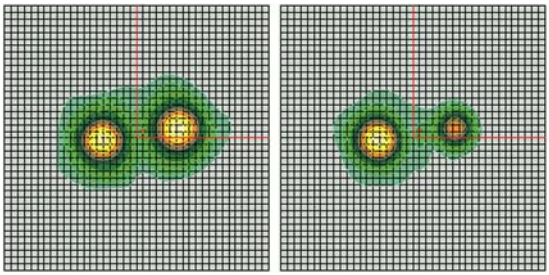

touching the source units, and consisted of 41 × 41 points with 1 cm spacing. The source model mesh was similar to the calculation mesh, but shifted 1.5 cm away from the array and extended by six rows/columns in all four directions.

Figure 13 shows contour plots of the reconstructed sound intensity for the two 1/3-octave bands at 4 and 5 kHz. WBH was applied to FFT spectra with 32 Hz line spacing, and 1/3 octaves were then synthesized. The significant level difference between the two source units in the 5 kHz band was consistent with beamforming processing of the same array data and with the intensity maps from the intensity probe scan.

Fig. 14. Comparison of narrow-band sound power spectra from the intensity probe scan and from WBH processing of the array data

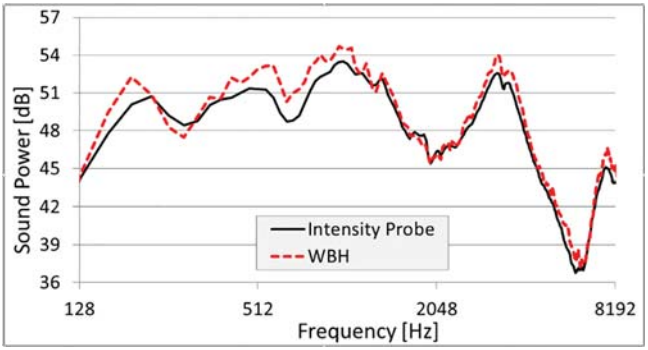

Figure 14 compares the sound power spectrum from the intensity probe scan with the sound power spectrum from the WBH reconstruction. Both were obtained by area integration of sound intensity maps. However, where the WBH map covers a relatively large area in the source plane, the intensity probe map covers a rather limited area at 7 cm distance. Consequently, the WBH result will be an

estimate of the total sound power radiated to a hemisphere, while the intensity-probe result will include only a part of that power. The generally slightly higher level of the WBH spectrum in Figure 14 should therefore be expected. The part of the WBH spectrum below approximately 1 kHz was obtained using standard ESM, so the iterative WBH algorithm seems to provide more accurate sound power estimates than standard ESM. As a conclusion, the sound power estimates from WBH are very accurate.

6. Conclusion

An iterative algorithm has been described for sparsity promoting NAH over a wide frequency range based on the use of an optimized pseudo-random array geometry. The method, which is called WBH, can be seen as an example of CS. The algorithm has been tested by a series of simulated measurements on point sources and on a plate in a baffle. Very good results were in general obtained at frequencies up to four times the normal upper limiting frequency for use of the particular array with holography. The focus has been on the ability to locate and quantify the main sources (source areas) in terms of sound power within approximately a 10 dB dynamic range. The method was found to work surprisingly well with distributed sources, such as vibrating plates. Typical application areas could be engines and gearboxes, where measurements at close range are often not possible, and the method seems to work very well at the distances that are typically realistic in such applications.

The iterative WBH algorithm was shown to provide sound field reconstructions almost identical to those of a conventional CS algorithm, where an optimization problem must be solved, involving minimization of the 1-norm of the solution vector. In the present work, such optimization problems have been solved using the CVX Matlab toolbox. For all the considered examples, the computation time of the CVX-based method was approximately 30 times longer than that of the iterative WBH method. In addition, the stopping criteria of the iterative WBH algorithm support the reconstruction of a large dynamic range without the risk of introducing numerical instability. This is not possible in the CVX-based approach, where a fixed dynamic range must be specified.

It was shown in the present paper that it may be advantageous to supplement both the CVX and the WBH algorithms with typically a standard ESM algorithm at the lowest frequencies in order to avoid misleading ghost sources in super-resolution results.

Engine and gearbox measurements are characterized by having sources at different distances. The sensitivity of the WBH algorithm to sources located outside the assumed source plane was therefore investigated in [6]. In general, the estimation of sound power was found not to be sensitive to sources being within reasonable distances from the assumed source plane.

Appendix A

Steepest Descent Algorithm

From a current approximation $\mathbf{q}$ to the complex source-model amplitudes, we wish to find the step length s in the direction $\mathbf{w}$ of steepest descent for the squared residual function F. The steepest descent direction is just the negative gradient of F:

$$\mathbf{w} \equiv -\nabla F(\mathbf{q}) = \mathbf{A}^H(\mathbf{p} - \mathbf{A}\mathbf{q}) = \mathbf{A}^H\mathbf{r}\,, \tag{A1}$$

$\mathbf{r}$ being the residual vector. In the calculation of s we need also the vector $\mathbf{g}$ defined as:

$$\mathbf{g} \equiv \mathbf{A}\mathbf{w}\,. \tag{A2}$$

Using these quantities and the definition of F in Eq. (10) we get after some manipulation:

$$F(\mathbf{q} + s\mathbf{w}) = \frac{1}{2}[s^2\mathbf{g}^H\mathbf{g} - 2s\mathbf{w}^H\mathbf{w} + \mathbf{r}^H\mathbf{r}]\,. \tag{A3}$$

From Eq. (A3), the step length s to the minimum of F along the direction $\mathbf{w}$ can be easily found by setting the derivative of $F(\mathbf{q}+s\mathbf{w})$ with respect to s equal to zero. As a result, we get:

$$s = \frac{\mathbf{w}^H\mathbf{w}}{\mathbf{g}^H\mathbf{g}}\,. \tag{A4}$$

So finally, the steepest descent step $\Delta\mathbf{q}$ is calculated as:

$$\Delta\mathbf{q} = s\mathbf{w}\,. \tag{A5}$$

Appendix B

Conjugate Gradient Algorithm

There is rich literature on such algorithms, see for example [13] and [14]. The algorithms solve a set of real or complex linear equations, where the coefficient matrix is positive definite and real symmetric or complex Hermitian. In order to bring the system of equations in Eq. (4) into a tractable form, we multiply by $\mathbf{A}^H$ on both sides, which leads to the Normal Equations:

$$\mathbf{A}^H\mathbf{p} = \mathbf{A}^H\mathbf{A}\mathbf{q}\,. \tag{B1}$$

Comparison with Eq. (11) shows that solution of Eq. (B1) is equivalent to finding the vector $\mathbf{q}$ for which the gradient of $F(\mathbf{q})$ equals zero:

$$\nabla F(\mathbf{q}) = -\mathbf{A}^H(\mathbf{p}-\mathbf{A}\mathbf{q}) = 0\,. \tag{B2}$$

The system of linear equations in Eq. (B1), with starting point obtained from the modified steepest descent algorithm, can be solved by application of the conjugate gradient algorithm.

References

[1] A. Sarkissian, "Method of superposition applied to patch near-field acoustical holography," J. Acoust. Soc. Am. **118**, 671–678 (2005).

[2] J. Hald, "Basic theory and properties of statistically optimized near-field acoustical holography," J. Acoust. Soc. Am. **125**, 2105-2120 (2009).

[3] J. Hald, "Scaling of plane-wave functions in statistically optimized near-field acoustic holography," J. Acoust. Soc. Am. **136**, 2687-2696 (2014).

[4] J. Hald, "Array designs optimized for both low-frequency NAH and high-frequency beamforming," *Proceedings of Inter-Noise 2004*, paper 425.

[5] G. Chardon, L. Daudet, A. Peillot, F. Ollivier, N. Bertin and R. Gribonval, "Near-field acoustic holography using sparse regularization and compressive sampling principles," J. Acoust. Soc. Am. **132**, 1521-1534 (2012).

[6] J. Hald, "Wideband acoustical holography," *Proceedings of Inter-Noise 2014*, paper 44.

[7] J. Hald, "Extension of acoustic holography to cover higher frequencies," *Proceedings of Automotive Acoustics Conference (Autoneum) 2015*, paper 20.

[8] International patent application no. PCT/EP2014/063597.

[9] T. Suzuki, "Generalized inverse beamforming algorithm resolving coherent/incoherent, distributed and multipole sources," *Proceedings of AIAA Aeroacoustics Conference 2008*, paper 2008-2954.

[10] J. Gomes and P. C. Hansen, "A study on regularization parameter choice in Near-field Acoustical Holography," *Proceedings of Acoustics'08 (Euronoise)*, 2875-2880 (2008).

[11] M. Grant and S. Boyd, "CVX: Matlab software for disciplined convex programming, version 2.1," *http://cvxr.com/cvx*, 2014

[12] E. G. Williams, *Fourier Acoustics: Sound Radiation and Nearfield Acoustical Holography* (Academic Press, London, 1999).

[13] M. R. Hestenes and E. Stiefel, "Methods of Conjugate Gradients for Solving Linear Systems," Journal of Research of the National Bureau of Standards **49**, 409–436 (1952).

[14] V. Frayssé and L. Giraud, "A set of conjugate gradient routines for real and complex arithmetics," CERFACS Technical Report TR/PA/00/47 (2000).

Evaluation of SPC and BSS for Indoor Pass-by Noise Contribution Analysis

A. Schuhmacher, E. Varricchio

Abstract

Indoor vehicle pass-by tests simulate field pass-by noise measurements. They are performed in a controlled environment and produce repeatable measurements that are independent of weather conditions. During vehicle development, indoor testing allows design modifications to be tested quickly in order to determine their immediate influence on the vehicle's overall noise levels. Besides pass-by noise tests, vehicle improvement requires knowledge about the noise contribution from different sources within the vehicle. In this article, a source path contribution (SPC) concept that involves modelling the main sources of pass-by noise during indoor vehicle tests is presented. A special feature of this approach is that it processes entirely within the time-domain to produce noise strength estimates for each of the considered sources. The estimates are then synthesized to produce pass-by noise estimates for the vehicle and for the individual noise sources. These estimates are based on indicator microphone near-field data and acoustic transfer functions. As a result, major pass-by noise contributors are identified for the vehicle at given positions during the pass-by test. Results produced by this method are compared to a blind source separation (BSS) methodology applied to the operational dataset for extracting source signals related to the different noise processes during vehicle operation. Extracted source signals are correlated with far-field measurements to estimate pass-by noise contributions. The BSS methodology is verified using a speaker set-up showing excellent separation of tyre and engine noise contributions. Data from indoor pass-by noise measurements with a vehicle on a chassis-dynamometer is finally used to test and evaluate the two methods.

Résumé

Les techniques de mesure de bruit de passage sur véhicule statique, mises en œuvre en chambre d'essais, simulent les émissions sonores au passage d'un véhicule roulant sur une piste d'essai en extérieur. Dans cet environnement

contrôlé, hautement reproductibles, ces mesures ne sont pas tributaires des aléas climatiques. Pendant la phase de conception d'un véhicule, cette méthode de mesure en intérieur permet de tester rapidement les modifications effectuées et d'en constater immédiatement les répercussions sur le niveau sonore global. Outre les essais de bruit de passage, les modifications doivent aussi prendre en compte les contributions de différentes sources sonores à l'intérieur du véhicule. Dans cet article est présentée une technique SPC (source path contribution) qui fait intervenir la modélisation des principales sources de bruit de passage dans le cadre de mesures en intérieur sur véhicule statique. Une des spécificités de cette approche est qu'elle est entièrement réalisée dans le domaine temporel et fournit une estimation des contributions de chacune des sources considérées. Les estimations ainsi obtenues sont ensuite synthétisées pour produire des valeurs de bruit de passage, tant pour le véhicule en tant que tel que pour chaque source prise individuellement. Ces estimations se basent sur des données de champ proche fournies par des microphones de mesure ainsi que sur des fonctions de transfert acoustique. Les principales contributions au bruit de passage du véhicule sont identifiées à des positions connues au cours de l'essai. Les résultats obtenus au moyen de cette méthode sont ici comparés à ceux d'une méthodologie BSS (blind source separation) appliquée à un jeu de données opérationnelles en vue d'extraire les signaux source liés aux processus sonores générés par un véhicule en fonctionnement. Ces estimations de bruit de passage sont corrélées avec des mesures en champ lointain. La méthodologie BSS est vérifiée au moyen d'un montage de haut-parleurs montrant une excellente séparation entre les contributions sonores des pneumatiques et celles du moteur. Enfin, le résultat des mesures de bruit de passage réalisées en intérieur sur un véhicule statique est utilisé pour évaluer les deux méthodes.

Zusammenfassung

Mit Messungen des Vorbeifahrgeräusches von Fahrzeugen in einer Akustikhalle (Indoor Pass-by noise testing) wird die Messung auf Teststrecken im Freien simuliert. Die Messungen in der Halle erfolgen unter kontrollierten Umgebungsbedingungen und ergeben reproduzierbare Messwerte, die von Wetterbedingungen unabhängig sind. Bei der Fahrzeugentwicklung ermöglichen Messungen in der Halle die schnelle Überprüfung von Designmodifikationen, um deren unmittelbaren Einfluss auf den Gesamtgeräuschpegel des Fahrzeugs zu bestimmen. Neben Vorbeifahrtgeräuschmessungen erfordert die Fahrzeugverbesserung auch Kenntnisse über die Beiträge verschiedener

Teilschallquellen zum Gesamtgeräusch des Fahrzeugs. In diesem Artikel wird ein Source Path Contribution-Konzept (SPC) vorgestellt, das die Modellierung der wichtigsten Geräuschquellen bei der simulierten Vorbeifahrt von Fahrzeugen in der Halle einbezieht. Eine Besonderheit dieses Ansatzes besteht darin, dass die Verarbeitung ausschließlich im Zeitbereich erfolgt, um die Stärke aller betrachteten Schallquellen abzuschätzen. Die Schätzwerte werden synthetisiert, um Werte für das Vorbeifahrgeräusch für das Gesamtfahrzeug und die einzelnen Schallquellen zu erhalten. Die Abschätzungen beruhen auf Nahfeldmesswerten von Indikatormikrofonen sowie akustischen Übertragungsfunktionen. Hiermit werden wesentliche Beiträge zum Vorbeifahrtgeräusch des Fahrzeugs an gegebenen Positionen während der Vorbeifahrtmessung identifiziert. Die mit dieser Methode erhaltenen Ergebnisse werden mit einer Blind Source Separation-Methodik (BSS) verglichen, die auf den operativen Datensatz angewendet wurde, um Schallquellensignale zu extrahieren, die sich auf die verschiedenen Geräuschprozesse während der Fahrt beziehen. Die extrahierten Schallsignale werden mit Fernfeldmessungen korreliert, um die Beiträge zum Vorbeifahrgeräusch abzuschätzen. Die BSS-Methodik wird mit einer Lautsprecheranordnung verifiziert, die eine ausgezeichnete Trennung der Beiträge von Reifen und Motor liefert. Schließlich werden Daten von Vorbeifahrtgeräuschmessungen in der Halle mit einem Fahrzeug auf einem Rollenprüfstand verwendet, um die beiden Methoden zu testen und auszuwerten.

1. Introduction

Indoor vehicle pass-by noise applications deal with measuring the exterior noise of a vehicle that is fixed on a chassis dynamometer (dyno) inside a large semi-anechoic room. During a standardized acceleration test, the noise is measured with an array of microphones placed in the vehicle far field, and the overall noise level versus vehicle position is determined. As such the indoor test is a simulated pass-by noise measurement. Since the indoor facilities allow controlled and repeatable measurements independent of weather conditions, this test is popular during the development stage of vehicle design allowing modifications to be tested out in a fast manner.

In addition to performing the indoor pass-by noise test, there is a growing need for vehicle noise-source contribution analysis. A source path contribution (SPC) concept is presented involving modelling the main vehicle noise sources contributing to the pass-by noise. The SPC methodology presented here processes

entirely in the time domain,working on measured time recordings during the fast acceleration test. Initially near-field microphone recordings are filtered to produce source-strength estimates for the considered noise sources followed by another set of synthesis filters to produce pass-by noise estimates for the vehicle and for individual noise sources. As a result we may identify major noise source contributions at given positions during the pass-by test.

For testing and validating the proposed methodology indoor pass-by noise measurements were carried out with a passenger car on a chassis dyno. In addition to a pass-by array of microphones in the far field, extra indicator microphones are placed near the noise sources of the test vehicle during the test. The indicator microphone data recorded during the acceleration test and transfer function data measured as frequency response functions (FRFs) using a small volume velocity source are combined to form a vehicle source model. A further synthesis process allows the prediction of exterior pass-by noise from the vehicle source model. The predicted pass-by result from the complete-vehicle SPC model are then compared with the indoor pass-by result obtained directly from the pass-by array of microphones to validate the SPC model setup.

Individual component source contributions are, however, more difficult to validate for an operating vehicle. In this study, a new operational source separation methodology based on blind source separation (BSS) is introduced briefly and verified for a simple setup using speaker signals. Next, the BSS approach is tested on data taken with the car on the chassis dyno to separate tyre noise from engine related noise, and finally, the pass-by contribution analysis is performed. Results from the SPC and BSS approach are compared and discussed.

2. Indoor Simulated Pass-by Noise Measurement

A pass-by noise measurement is defined as the method of measuring the noise emission of an accelerating road vehicle at various gear positions in a certain measurement range. These measurements are mandatory for automotive manufacturers in terms of product certification. For this reason, the International Organization for Standardization (ISO) regulates the measurement and analysis procedures, as well as the reporting format [1].

In some cases, however, pass-by noise measurements cannot be taken in the field because of bad weather or poor test-track conditions. In such cases, an indoor simulation of a pass-by noise measurement is often used. The simulation offers a number of advantages such as good repeatability, flexibility and ease of use. It is

Fig. 1. Field pass-by and indoor simulated pass-by noise measurement

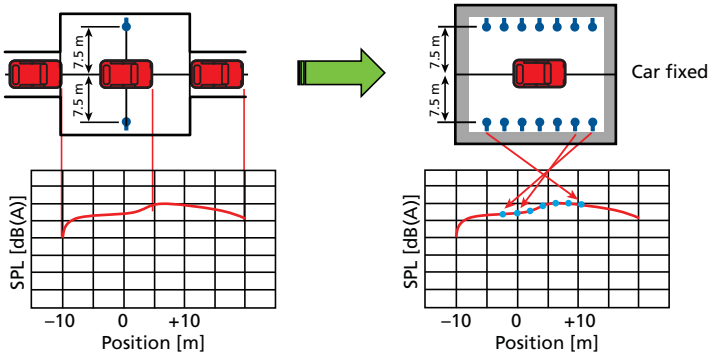

being considered as the conformance test, together with the field pass-by test, by ISO standard.

Instead of driving the test vehicle past two stationary microphones, as is the standard procedure in a field pass-by measurement, indoor pass-by test setups use one or two rows of microphones placed alongside the vehicle. See Figure 1 for a comparison of the field and indoor situation. The vehicle runs on a chassis dyno and is accelerated as it would be for a field pass-by measurement. Time histories are measured by the microphones together with vehicle parameters and dyno drum speed. A sophisticated algorithm uses the information from the dyno to calculate the vehicle's position relative to the microphones as a function of time. This is used to extract the contributing portions of the time histories that correspond to when the vehicle would have passed the standard microphone positions had it been moving. A single synchronized time history is created by stitching all of these time history sections together and interpolating across the segments' boundaries. This synchronized single-time record combined with the dyno drum speed profile represents the vehicle noise emitted during a simulated pass-by measurement. The new time history is played back through the analysis section of the system, offering the option of applying various types of frequency analysis to the time history. It can also be previewed and listened to in order to determine whether it sounds right.

The indoor pass-by system described in this paper has been developed to allow for microphone positions closer than 7.5 m from the vehicle while still providing correct results. This is extremely useful for situations where space is limited and is achieved by assuming that the noise is emitted from one point (an acoustic center) as seen from the far-field. Individual acoustic centers can be chosen for the left and

the right side of the vehicle. In addition, the array of microphones does not need to have full coverage of all vehicle positions since typically the room size is limited. Missing microphone positions close to the entrance or exit of the virtual pass-by track can be simulated from the existing array microphones and the specified acoustic centers. This latter feature is employed in this study.

3. Contribution Analysis Methods

3.1. SPC Modelling of Noise Sources

In order to estimate contributions from the different vehicle noise components, more effort is typically required. The classic approach is to apply acoustic transfer path analysis [2, 3] (called SPC here) which is based on a solid foundation. All relevant noise components are modelled using a set of acoustic point sources, their source strength during operation is calculated from near-field acoustic data and FRFs. Finally, the source strengths are propagated to the receiver via other acoustic FRFs. In the current context, the receivers would be the array of microphones for the indoor simulated pass-by test. The near-field data is measured using indicator microphones at selected positions close to any vehicle noise source, that is inside engine room, close to mufflers, exhaust and tyres. The classical approach has been extended to time-domain simply working directly on the recordings measured by the indicator microphones and applying time filters derived from the FRFs. The procedure for performing such analysis has been reported earlier [4], but is briefly reviewed in the following.

Fig. 2. SPC modeling of vehicle noise sources for indoor pass-by contribution analysis

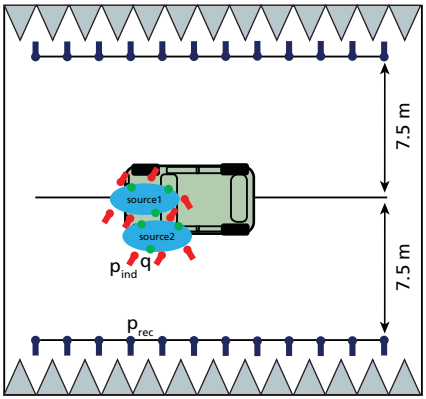

In Figure 2, a vehicle setup is shown involving two noise sources modelled by a set of distributed point sources. Indicator microphones are placed close to the chosen point sources, and by measuring every acoustic FRF between any point source and all indicator positions we may be able to deal with the problem of crosstalk, that is an indicator microphone close to source 2 measures a mixture of both source 1 and source 2 contributions. The cancellation of any crosstalk is however very dependent on the chosen point source models and the quality of the measured FRFs. The FRF matrix between point sources and indicators is inverted and turned into inverse filters. Indicator recordings during pass-by acceleration are filtered by the matrix of inverse filters to get source strength time histories for every point source in the model.

$$\boldsymbol{q}_{src}(t) = \boldsymbol{H}(t) \otimes \boldsymbol{p}_{ind}(t) \tag{1}$$

Here $\boldsymbol{H}(t)$ is an $n \times m$ matrix of sufficiently long inverse filters (convolved with $\boldsymbol{p}_{ind}(t)$)where n is the number of point sources in the model and m is the number of indicator microphones.

The contribution from each component source to one of the receiver microphones of the pass-by array is found by adding the corresponding point sources:

$$p_{rec}(t) = \sum g(t) \otimes q_{src}(t), \tag{2}$$

where g(t) is another time filter from source to receiver made from the measured FRF, and the sum is taken over the set of point sources belonging to a component source. Repeating this for every component source and every receiver microphone results in predicted contributions all synchronized with the indicator recordings and the corresponding vehicle speed. Pass-by noise contributions are calculated using the indoor simulated pass-by algorithm on the contribution time data for the pass-by array.

As opposed to considering the full matrix $\boldsymbol{H}$ of all source positions and all indicator positions in the same matrix, and as such model all possible crosstalk between noise source components, a component submatrix solution approach can be used to model only the relevant crosstalk. For example, when engine noise is strong compared to front-tyre noise, engine noise crosstalk will appear at the front tyre indicator microphones but very little front-tyre noise contribution will appear

at the engine indicator microphones inside the engine room. In that situation we should only allow for removal of engine noise contribution at the front-tyre indicators. This is controlled by solving a set of smaller submatrix problems in an appropriate sequence. Additionally, by considering only small component FRF matrices, numerical issues with matrix inversion becomes less severe since the matrix condition numbers are much smaller. The important thing though, is to make the correct sequence of matrix solutions in order to remove relevant crosstalk only. Figure 3 shows one such sequence indicating that as a first step the source 1 component source strengths are found from corresponding indicator microphone sound pressures, $\boldsymbol{p}_{source1}(t)$, and the local FRFs for that source only. Next, the source 1 contributions are subtracted from source 2 indicator sound pressures. The source strengths for source 2 are estimated with the modified source pressures, $\tilde{\boldsymbol{p}}_{source2}(t)$, and the local FRFs for that component source. This is repeated until all component source strengths are estimated. The stronger noise sources should therefore appear at the beginning of the sequence. Pass-by noise contributions are obtained from the estimated component source strengths, propagated to the pass-by array microphones, and finally indoor simulated pass-by calculations are performed.

Fig. 3. Example of submatrix solution sequence for estimating volume velocity source strengths for setup in Figure 2 and eventually predict pass-by noise contributions

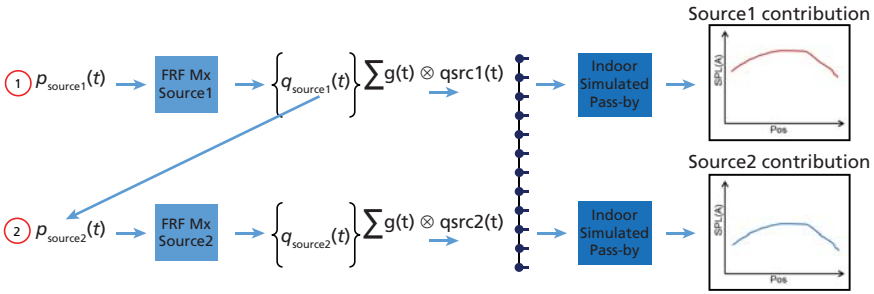

3.2. Blind Source Separation Approach

BSS refers to signal processing methods with the aim of separating different source signals from a mixture of sources using little information about the source signals and the mixing process. In acoustics the mixing process of different sources at sensors is complicated by the fact that the propagation is convolutive due to delays and reflections between sources and sensors. Many different methods have been proposed in the past to solve the separation problem at the sensors. Most methods focused on music and speech related problems, and

algorithms working in either frequency domain or time domain are reported. BSS on industrial types of signals is however rarely found. Most methods make the assumption that the source signals are independent and other signal properties like non-stationarity may also be exploited [5]. For the current problem of separating vehicle noise sources during a fast acceleration, a time-domain method for separating microphone recordings into so-called independent components (ICs) is employed. The basic principle of the selected separator is to make use of a linear prediction approach to model the time correlations of a set of recorded mixtures, here called reference signals $\boldsymbol{p}_{ref}(t)$. A matrix of whitening filters $\boldsymbol{W}(t)$ can be estimated from the correlations to produce a set of whitened signals, $\boldsymbol{u}(t)$.

$$\boldsymbol{u}(t) = \boldsymbol{W}(t) \otimes \boldsymbol{p}_{ref}(t) \tag{3}$$

The feature of $\boldsymbol{u}(t)$ is that the samples of each signal $u_i(t)$ are now uncorrelated. The final step is to solve an instantaneous BSS problem looking for a matrix $\boldsymbol{B}$ which rotates the whitened data to find the most independent time series, the ICs in the vector of time series $\boldsymbol{y}(t)$. Standard algorithms may be applied here using either higher-order or second-order statistics.

$$\boldsymbol{y}(t) = \boldsymbol{B} \cdot \boldsymbol{u}(t) \tag{4}$$

Such a two-stage linear prediction approach for solving the convolutive BSS problem has been proposed for blind identification of communication channels [6] and other variants of this implementation for source separation are reported as well [7].

Having separated into ICs, contribution filters can be estimated using time recordings at the desired receiver microphones which had been measured together with the set of reference microphones.

3.2.1. Validation of BSS for engine and tyre noise separation

In order to demonstrate the capabilities of the chosen BSS strategy for noise source separation, a simple yet challenging experimental test setup was considered. A small vehicle located in a normal room served as scattering object and two speakers were positioned around the vehicle. One box loudspeaker on the floor at the right-hand side of the vehicle and a tyre structure with built-in speaker was positioned at the rear left side of the vehicle. A set of 4 reference microphones were mounted on the floor in positions between the two considered speaker

Fig. 4. Two-speaker setup around small vehicle for evaluation of BSS separation. Reference microphones are placed close to the speakers and a set of far-field microphones serve as pass-by receivers. The microphones marked with a circle are used in the validation study presented here

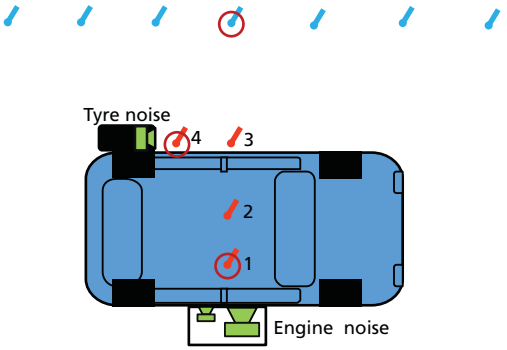

sources, in addition to an array of microphones placed along the vehicle left side to represent a set of pass-by receivers. The setup is sketched in Figure 4.

Real recordings from another measurement served as input for the two speaker sources. An engine signal consisting of engine orders only was sent to the box speaker to produce pure engine noise, and another signal, made by a recorded tyre signal with all engine orders removed, was sent to the tyre speaker to represent pure tyre noise. Both recordings were originally taken during a pass-by acceleration test, and after modification they are considered as independent signals making them amenable for BSS analysis. All time recordings for this validation case were done using a sampling frequency of 32768 Hz and about 12 seconds of data was recorded.

By playing the two signals simultaneously through the speakers, mixtures are created at the microphones in the setup, as would be the case during a real vehicle operating. The advantage of the setup is that each speaker can play solo to create the true contributions at the microphones for validation purposes. The convolutive mixture of the tyre and engine signals as picked up by the two reference microphones closer to the speakers, that is reference #1 and reference #4 are used in the adaptive blind separation stage to generate two new signals which are independent. The independent signals are not associated with any particular position from the setup and the order in which they appear at the output of the unmixing process is arbitrary. So to make meaningfull use of the independent signals it is necessary to identify which noise source process each IC belongs to.

Fig. 5. ***Left****: Spectrogram of engine/tyre mixture at reference #4.* ***Centre****: Contribution of separated ICs at reference #4.* ***Right****: True measured tyre and engine contributions at reference #4*

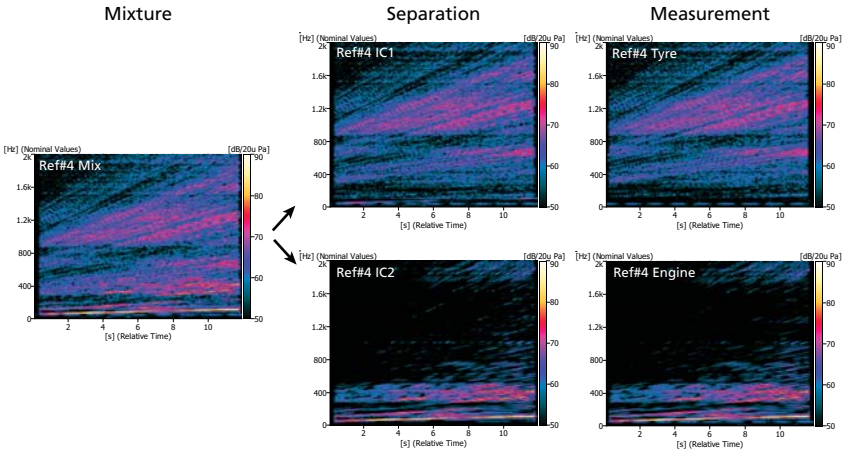

Before processing the measured reference microphone mixtures, the data samples were down-sampled with a factor 2 to reduce the number of samples and possibly reduce the length of the unmixing filters. This so-called sub-band processing is a standard BSS procedure and after processing the time data can be up-sampled again [8]. Note, if the data is split into several subbands for processing, ICs belonging to different subbands must be combined to form the full-band signals again, but since the IC order is unknown for each subband this associated permutation problem must be solved. In our case only one subband is considered so this permutation problem is not an issue. Next, the unmixing filters are trained using the 12 seconds of data, that is the whitening filters are constructed and the data whitened followed by solving an instantaneous problem. The only parameter set is the filter length of the whitening filters. The output of this procedure is two IC time signals, which are filtered versions of the clean reference signals related to either of the two speakers. The ICs are now correlated with the input signals (reference #1 and reference #4) to calculate a set of time filters between ICs and the two reference microphones. Finally, we can transform each IC into a time-domain contribution at a reference microphone, which re-scales each IC back to sound pressure at the physical microphone positions. Results for this procedure in the given case are shown in Figure 5. The mixture of reference #4 close to the tyre speaker is shown as spectrogram, then the

*Fig. 6. Average spectrum at receiver #4. The sound mixture measurement (**black**) versus sum of contributions from IC's (**yellow**)*

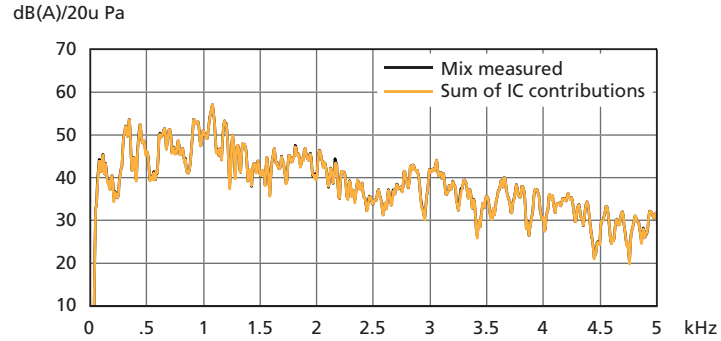

contribution of the two ICs at this reference microphone is shown next and for comparison, we include the true contributions from the engine speakers and the tyre speaker. We notice that IC 1 represents the tyre signal and IC 2 the engine signal, and furthermore we see impressive agreement between the BSS separated contributions and the true individually measured contributions. Only very little engine noise is left in the tyre noise estimations, and vice versa, suggesting that the separation problem has been solved.

The final step is to correlate the ICs found with the selected far-field receiver data measured simultaneously with the reference mixtures. Another set of filters are estimated from the ICs (input) to the receiver (output) and subsequently used to filter each IC to find the receiver contribution time signal. The average spectrum during the 12 seconds of measurement at receiver #4 is plotted together with the contribution from IC 1 (tyre) and IC 2 (engine). In Figure 6, the average spectrum is shown for the measurement at receiver #4 and compared with the sum of the two contributions from the ICs. We observe excellent agreement between the two

*Fig. 7. Average spectrum at receiver #4. Tyre speaker measured vs. contribution from IC 1 (**left**). Engine speaker measured vs. contribution from IC 2 (**right**)*

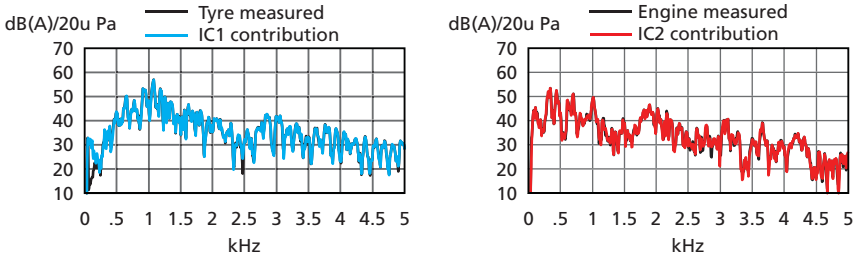

spectra, telling us that the two derived ICs fully describe the measured signal at the receiver. Moreover, in Figure 7 we plot the true measured average spectrum from each speaker against the IC contribution spectrum which is identified to represent the corresponding speaker. Again, near to perfect agreement is seen suggesting that the convolutive mixing problem has been solved satisfactorily.

4. Indoor Pass-by Measurement Setup

Fig. 8. Single-side indoor pass-by measurement set-up with additional indicator microphones for contribution analysis

A setup with a vehicle on a chassis dyno in an indoor pass-by test room is now considered. The test room could only accommodate a single-sided pass-by test with pass-by microphones at 7.5 m, hence all results presented in the following refer to the left side of the vehicle. The midsize passenger test vehicle was equipped with normal tyres making tyre contribution to pass-by noise significant. In total 25 indicator microphones were placed close to potential noise sources (engine, intake, mufflers, exhaust and tyres) of the vehicle and 20 source positions were distributed among these noise sources. The contribution from the right side tyres to the left side pass-by noise is neglected in this study, hence no indicator microphones were placed close to these tyres. 12 pass-by microphones covered the left side of the vehicle. The spacing between the pass-by microphones was 1 m for the microphones closer to the vehicle whereas the spacing of other microphones was 2 m. A picture of the single-sided indoor pass-by setup is shown in Figure 8.

Two separate measurement tasks must be completed to do the indoor pass-by test including the additional contribution analysis. For different pass-by conditions (acceleration and constant speed test), time data of all microphones in the setup and the required tachometer pulses were recorded with a sampling rate of 16384 Hz. Following the operational measurements, a volume velocity source was used to measure acoustic FRFs from a source position to all microphones in the setup. This was repeated for every source position of the vehicle SPC model. The frequency range considered for these tests was up to 6.4 kHz.

5. Pass-by Acceleration Results

An acceleration test in third gear is analysed using a dataset performed as described previously. The synchronization condition chosen here is 50 km/h at the center (x = 0 m) of the virtual pass-by track according to the new ISO 362 test procedure. From that condition the simulated pass-by time signal is constructed and turned into overall SPL(A) as a function of the vehicle position inside the virtual pass-by track. This process is carried out for the recordings made at the pass-by array microphones during the acceleration test and also for the source contributions resulting from the SPC analysis of the indicator microphone recordings and the corresponding FRFs. From the initial set of source and indicator positions, a subset was selected to avoid numerical problems during the calculation of source strengths. 24 indicator microphones and 15 source positions were used for the SPC contribution analysis and the component submatrix solution approach described earlier was adopted with an appropriate sequence to minimize the influence of crosstalk between source components. The result of summing all source contributions and comparing the sum with the indoor pass-by result can be used to verify that all pass-by noise contributors were picked up by the indicator microphones. Processing results for the acceleration operating condition are shown in Figure 9. Notice that the result is shown from vehicle position −10 m to +10 m although the pass-by microphones only covered the vehicle positions from roughly −4 m to +10 m, so the extrapolation capability of the indoor pass-by calculations has been used. We observe fine agreement between the indoor pass-by result and the sum of all contributors from the vehicle SPC model, that is all significant noise sources are included in the analysis. Individual contributions reveal dominating engine noise contribution to pass-by noise with intake and tyre noise contributing significantly as well. The exhaust outlet is a major contributor towards the exit of the pass-by track.

Fig. 9. Overall SPL(A) versus vehicle position for third gear acceleration pass-by test. Indoor pass-by results and source contributions from SPC vehicle model

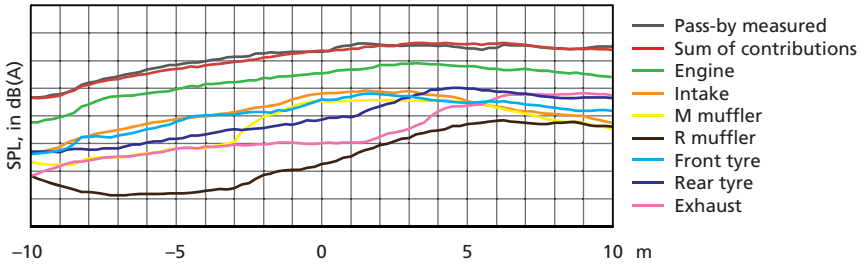

For a given vehicle position the 1/3 octave band levels can be investigated to see how the peak overall SPL(A) is composed. Figure 11 provides the 1/3 octave contribution levels at vehicle position +4 m. Acceptable agreement between what is measured by the pass-by microphones and the model prediction (Sum Contributions) is found. Engine contribution dominates most of the frequency bands with significant tyre contribution at higher frequencies, in particular in the 1 kHz band.

The SPC modeling of the vehicle revealed fine agreement between the noise prediction and the direct result from the pass-by microphones, however, the individual source contributions are by nature more difficult to validate. The attempt taken here will be to make use of the described blind separation technique to estimate the pass-by noise contribution from the front and the rear tyre, respectively, and compare with the SPC prediction.

The measured set of indicator recordings can serve as input data to the blind separation process of identifying a set of ICs for the noise processes during vehicle operation. In this study 23 reference microphones were selected from the 25 available indicator microphones. Two engine room indicator microphones were

Fig. 10. 1/3 octave contribution analysis corresponding to vehicle position +4 m during acceleration pass-by test. Indoor pass-by result and SPC source contributions

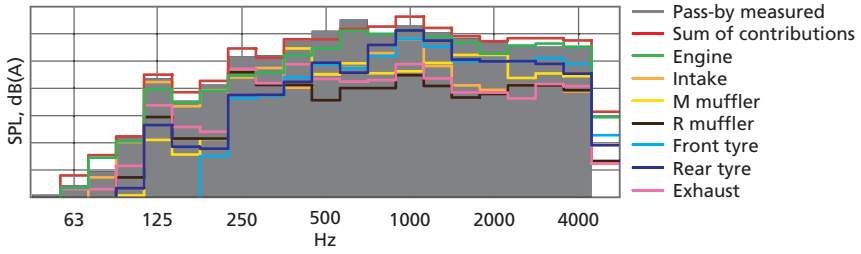

discarded. From the third gear acceleration recordings, 12 seconds of data were picked representing the run-up and coast-down part, and this time data was down-sampled to 8192 Hz to reduce the amount of data. In effect, only the frequency content up to 4096 Hz is considered. The blind separation of the 23 reference microphone channels results in 23 IC time signals which are sorted according to their power contribution at the 23 reference microphones thus making labelling possible. Three of the ICs were selected to represent noise processes caused by the front tyre and another three ICs represent the rear tyre. To understand if all 23 derived ICs can represent the measured noise at the pass-by microphones, the multiple-input/multiple-output problem between all IC signals and all pass-by microphone signals is solved to obtain a matrix of time filters. All 23 ICs can be filtered and summed at one of the pass-by microphones and we can compare it with the actual measured signals during the run-up and coast-down. The average spectrum comparison between the measurement and sum of all IC contributions is performed for pass-by microphone #5, see Figure 12. Below 1.6 kHz, all of the noise measured by the pass-by microphone is accounted for by the ICs, whereas at high frequencies, there is a small gap between what is measured and what is reconstructed by the ICs. However, the high frequencies are less important in the overall SPL(A).

*Fig. 11. Average SPL(A) spectrum at pass-by microphone #5 during third gear acceleration. Measurement (**black**) and sum of all IC contributions (**yellow**)*

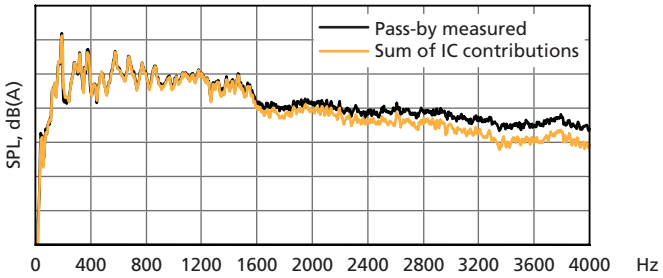

Having established the matrix of filters between each IC signal and each pass-by microphone, we can calculate and listen to the contribution from each IC at a pass-by microphone. Furthermore, the contributions of the three identified ICs for each of the two tyres are summed at every pass-by microphone and the resulting time signals are combined with the original tacho signal recordings for indoor simulated pass-by evaluation. As a result we get an estimate of the front tyre and the rear tyre pass-by noise contribution provided by the BSS approach. A

*Fig. 12. Overall SPL(A) vs vehicle position for third gear acceleration pass-by test. Indoor pass-by measured (**grey**) and tyre contributions estimated by SPC (**solid**) and BSS (**dashed**) methods for front and rear tyre*

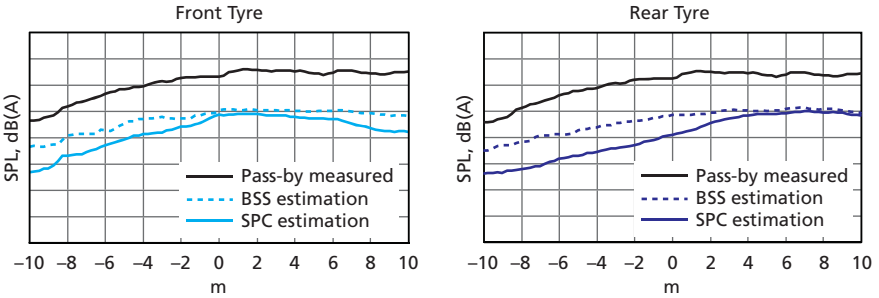

comparison of the predicted tyre contributions from the two methods considered is shown in Figure 13.

At vehicle positions where the tyres contribute the most to the pass-by noise we have comparable levels from the SPC and the BSS approach, with BSS providing higher levels in general. Figure 13 compares the 1/3-octave levels at vehicle position +4 m for the two tyres. The front tyre contributions for SPC and BSS are similar above 800 Hz whereas BSS shows more pronounced low-frequency content compared to SPC. The rear tyre contribution spectra are comparable.

*Fig. 13. 1/3 octave spectrum at +4 m during third gear acceleration pass-by test. The indoor pass-by measured (**grey**) and source contributions from SPC (**solid**) and BSS (**dashed**)*

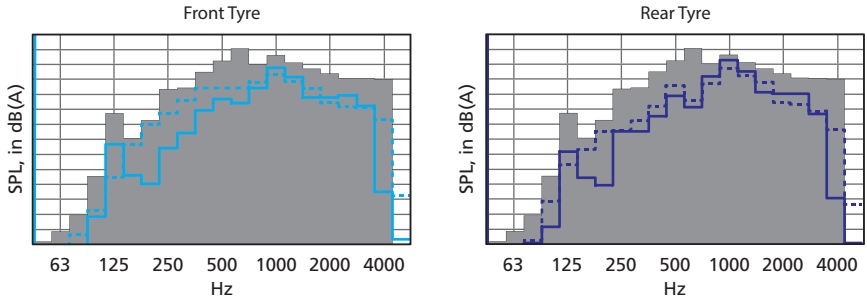

6. Pass-by Constant Speed Results

A third gear constant speed test (50 km/h) was processed and analysed in a similar fashion using the same source positions and indicator microphones for the SPC

model as for the acceleration case. The submatrix calculation was employed for estimating source strength time data with minimum crosstalk between noise source components. Here the submatrix solution sequence differed from the acceleration case since the crosstalk between components is different for each operating condition. The final SPC processing is though identical to the acceleration case and the obtained source contributions as overall SPL(A) during the pass-by test are plotted together with the indoor pass-by result in Figure 14. Fine correspondence between indoor pass-by result and sum of all source contributions is observed. For this test condition the engine and the two tyres mainly contribute to the total measured pass-by noise.

Fig. 14. Overall SPL(A) versus vehicle position for third gear constant speed pass-by test. Indoor pass-by results and source contributions

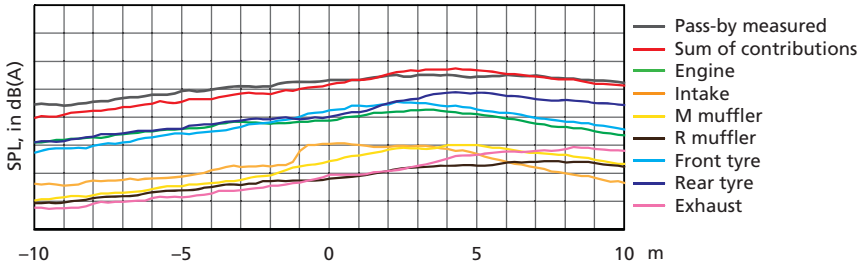

1/3-octave contribution results at vehicle position +4 m indicate that the pass-by noise at this position is dominated by the frequency content from 500 Hz to 2 kHz, and that the rear tyre is the main contributor, see Figure 15.

Fig. 15. 1/3 octave contribution analysis corresponding to vehicle position +4 m during constant speed pass-by test

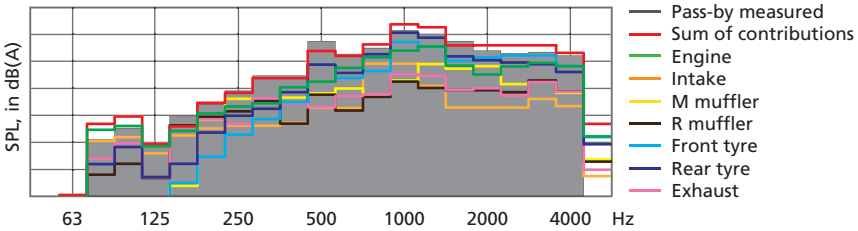

For verification, a blind separation of the operating time data at the same 23 reference microphones used for the acceleration case was performed using 12 seconds of data for each microphone. Down-sampling with a factor of two was again performed before blind separation into ICs. A few ICs were seen to

*Fig. 16. Average SPL(A) spectrum at pass-by microphone #5 during constant speed test. Measurement (**black**) and sum of all IC contributions (**yellow**)*

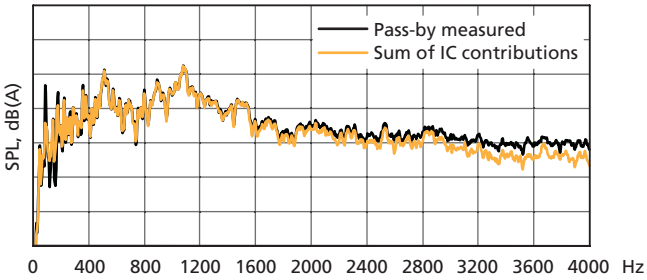

contribute almost exclusively to the noise measured with the indicator microphones close to each tyre, hence these ICs were selected to represent noise processes related to tyre noise generation. First of all, it is examined if the 23 obtained ICs can represent the measured noise at the pass-by microphones, and compare the spectrum of pass-by microphone #5 with the sum of contributions from all 23 ICs. In Figure 16 these two spectra are compared showing excellent agreement especially in the range between 400 Hz and 1.6 kHz where most of the signal power is present. Some low-frequency harmonics are less well reproduced by the sum of ICs, and at high frequencies, we see a small gap between spectra, indicating that more noise processes should be taken into account.

*Fig. 17. Overall SPL(A) versus vehicle position for constant speed pass-by test. Indoor pass-by measured (**grey**) and tyre contributions estimated by SPC (**solid**) and BSS (**dashed**) methods for front and rear tyre*

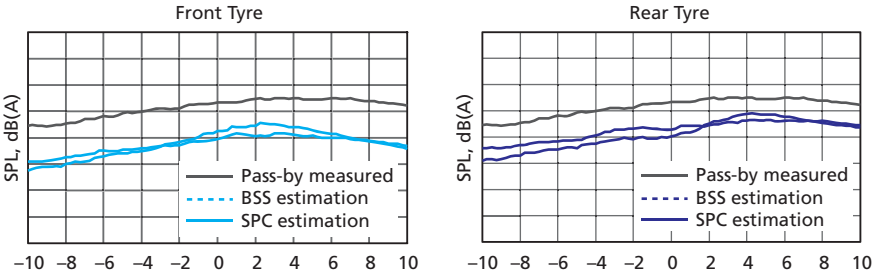

The two sets of ICs representing each of the two tyres are processed to obtain an estimate of their pass-by noise contribution, see Figure 17. For this condition, we see a reasonably good agreement between tyre noise estimates from SPC and BSS approaches over the whole pass-by track.

1/3 octave contribution spectra for vehicle position +4 m are compared in Figure 18 showing good agreement between front tyre contribution spectra in particular in the range 500 Hz to 2 kHz which is dominating the overall SPL(A). For rear tyre contribution spectra, the SPC model estimates rather high levels around 1 kHz matching the total measured spectrum levels. Otherwise we have good correspondence between SPC and BSS 1/3 octave levels.

*Fig. 18. 1/3 octave spectrum at +4 m during constant speed pass-by test. Indoor pass-by measured (**grey**) and source contributions from SPC (**solid**) and BSS (**dashed**)*

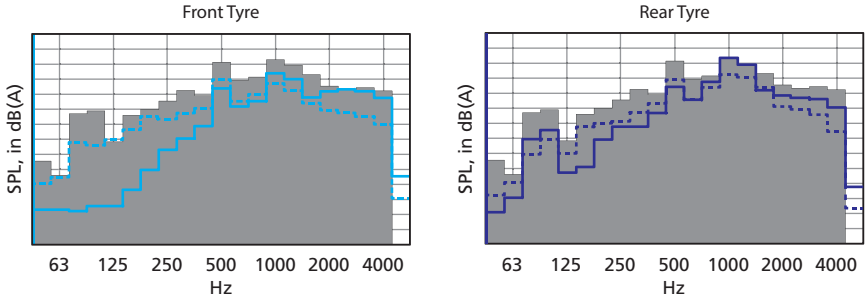

Conclusion

This paper has dealt with indoor vehicle pass-by noise measurements for performing noise source contribution analysis in addition to the more conventional overall simulated pass-by evaluation. A vehicle SPC model approach was considered for separating noise source components using indicator microphone operating data and measured FRFs. A component submatrix solution approach for estimating the source strengths of the vehicle SPC model was introduced. With this solution approach, relevant crosstalk between components is cancelled while the matrix inversion becomes more straightforward. The predicted pass-by noise from the vehicle SPC was compared with the indoor simulated pass-by result to verify the sum of all modelled contributions. Good correspondence was found for both the acceleration test and the constant speed test. Individual source contributions are harder to verify, the attempt described here was to use a new operational BSS technique for decomposing into at least individual tyre and engine-related noise contributions. Considering the assumptions in SPC and BSS, fine agreement between predicted tyre pass-by noise contributions were found. The BSS approach for noise source separation will be explored in more detail to determine how many reference microphones are needed to have adequate

separation of vehicle noise sources. Further validations of both methods for accurate contribution analysis will be carried out.

References

[1] ISO 362, Acoustics – Measurement of noise emitted by accelerating road vehicles – Engineering method, International Organization for Standardization (ISO).

[2] J. W. Verheij, *Inverse and reciprocity methods for machinery noise source characterization and sound path quantification. Part 1: Sources*, Int. Journal of Acoustics and Vibration, Vol. 2, No.1, (1997), pp. 11-20.

[3] J. W. Verheij, *Inverse and reciprocity methods for machinery noise source characterization and sound path quantification. Part 2: Transmission Paths*, Int. Journal of Acoustics and Vibration, Vol. 2, No.3, (1997), pp. 103-112.

[4] A. Schuhmacher, Y. Shirahashi, M. Hirayama, Y. Ryu, *Indoor pass-by noise contribution analysis using source path contribution concept, Proceedings of the 2012 International Conference on Modal Analysis Noise and Vibration Engineering (ISMA),* Leuven (2012), pp. 3697-3709.

[5] P. Comon, C. Jutten, *Handbook of blind source separation,* Academic Press, New York (2010).

[6] K. Abed-Meraim, E. Moulines, *Prediction error method for second-order blind identification*, IEEE Trans. Signal Processing, Vol. 45, No. 3, (1997), pp. 694-705.

[7] L.K. Hansen, M. Dyrholm, *A prediction matrix approach to convolutive ica*, in C. Molina et al. (ed.), *Proceedings of IEEE Workshop on Neural Networks for Signal Processing XIII*, Toulouse (2003), pp. 249-258.

[8] K. Kokkinakis, P. Loizou, *Subband-based blind signal processing for source separation in convolutive mixtures of speech*, *Proceeding of IEEE International Conference on Acoustics, Speech and Signal Processing*, Honolulu (2007), pp. 917-920.

Previously issued numbers of Brüel & Kjær Technical Review

(Continued from cover page 2)

	Use of FE Models in the Optimisation of Accelerometer Designs
	System for Measurement of Microphone Distortion and Linearity from Medium to Very High Levels
1 – 2001	The Influence of Environmental Conditions on the Pressure Sensitivity of Measurement Microphones
	Reduction of Heat Conduction Error in Microphone Pressure Reciprocity Calibration
	Frequency Response for Measurement Microphones – a Question of Confidence
	Measurement of Microphone Random-incidence and Pressure-field Responses and Determination of their Uncertainties
1 – 2000	Non-stationary STSF
1 – 1999	Characteristics of the vold-Kalman Order Tracking Filter
1 – 1998	Danish Primary Laboratory of Acoustics (DPLA) as Part of the National Metrology Organisation
	Pressure Reciprocity Calibration – Instrumentation, Results and Uncertainty
	MP.EXE, a Calculation Program for Pressure Reciprocity Calibration of Microphones
1 – 1997	A New Design Principle for Triaxial Piezoelectric Accelerometers
	A Simple QC Test for Knock Sensors
	Torsional Operational Deflection Shapes (TODS) Measurements
2 – 1996	Non-stationary Signal Analysis using Wavelet Transform, Short-time Fourier Transform and Wigner-Ville Distribution
1 – 1996	Calibration Uncertainties & Distortion of Microphones.
	Wide Band Intensity Probe. Accelerometer Mounted Resonance Test
2 – 1995	Order Tracking Analysis

Special technical literature

Brüel & Kjær publishes a variety of technical literature that can be obtained from your local Brüel & Kjær representative.

The following literature is presently available:

- Catalogues
- Product Data Sheets

Furthermore, back copies of the Technical Review can be supplied as listed above. Older issues may be obtained provided they are still in stock.

Front cover: Offshore wind turbines near the coast of Denmark

Each Brüel & Kjær Technical Review contains a collection of technical, scientific articles that describe theory, measurement techniques and instrumentation, which are specifically aimed at acousticians and vibration engineers.

See more on **bksv.com/library**, Technical Reviews

BV 0066 – 11 2014-11

Brüel & Kjær Sound & Vibration Measurement A/S
DK-2850 Nærum · Denmark · Tel: +45 77 41 20 00 · Fax: +45 45 80 14 05
www.bksv.com · info@bksv.com
Local representatives and service organisations worldwide